Title	An experimental and kinetic modeling study of the ignition delay characteristics of binary blends of ethane/propane and ethylene/propane in multiple shock tubes and rapid compression machines over a wide range of temperature, pressure, equivalence ratio, and dilution
Author(s)	Martinez, Sergio; Baigmohammadi, Mohammadreza; Patel, Vaibhav; Panigrahy, Snehasish; Sahu, Amrit B.; Nagaraja, Shashank S.; Ramalingam, Ajoy; Mohamed, A. Abd El-Sabor; Somers, Kieran P.; Heufer, Karl A.; Pekalski, Andrzej; Curran, Henry J.
Publication Date	2021-03-02
Publication Information	Martinez, Sergio, Baigmohammadi, Mohammadreza, Patel, Vaibhav, Panigrahy, Snehasish, Sahu, Amrit B., Nagaraja, Shashank S., Ramalingam, Ajoy, Mohamed, A. Abd El-Sabor, Somers, Kieran P., Heufer, Karl A., Pekalski, Andrzej, Curran, Henry J. (2021). An experimental and kinetic modeling study of the ignition delay characteristics of binary blends of ethane/propane and ethylene/propane in multiple shock tubes and rapid compression machines over a wide range of temperature, pressure, equivalence ratio, and dilution. Combustion and Flame, 228, 401-414. doi:https://doi.org/10.1016/j.combustflame.2021.02.009
Publisher	Elsevier
Link to publisher's version	https://doi.org/10.1016/j.combustflame.2021.02.009
Item record	http://hdl.handle.net/10379/16953
DOI	http://dx.doi.org/10.1016/j.combustflame.2021.02.009

Combustion and Flame 228 (2021) 401–414

Contents lists available at ScienceDirect

Combustion and Flame

journal homepage: www.elsevier.com/locate/combustflame

An experimental and kinetic modeling study of the ignition delay characteristics of binary blends of ethane/propane and ethylene/propane in multiple shock tubes and rapid compression machines over a wide range of temperature, pressure, equivalence ratio, and dilution

Sergio Martinez[a], Mohammadreza Baigmohammadi[a], Vaibhav Patel[a], Snehasish Panigrahy[a,*], Amrit B. Sahu[a], Shashank S. Nagaraja[a], Ajoy Ramalingam[b], A. Abd El-Sabor Mohamed[a], Kieran P. Somers[a], Karl A. Heufer[b], Andrzej Pekalski[c], Henry J. Curran[a,*]

[a] Combustion Chemistry Centre, School of Chemistry, Ryan Institute, MaREI, NUI Galway, University Road, Galway H91 TK33, Ireland
[b] Physico-Chemical Fundamentals of Combustion, RWTH Aachen University, 52056 Aachen, Germany
[c] Shell Research Limited, Shell Centre London, London SE1 7NA, United Kingdom

ARTICLE INFO

Article history:
Received 12 November 2020
Revised 4 February 2021
Accepted 8 February 2021
Available online 2 March 2021

Keywords:
Ethane
Ethylene
Propane
Shock-tube
Rapid compression machine
Ignition delay time

ABSTRACT

In this work, the ignition delay time characteristics of C_2 – C_3 binary blends of gaseous hydrocarbons including ethylene/propane and ethane/propane are studied over a wide range of temperatures (750 – 2000 K), pressures (1 – 135 bar), equivalence ratios (φ = 0.5 – 2.0) and dilutions (75 – 90%). A matrix of experimental conditions is generated using the Taguchi (L_9) approach to cover the range of conditions for the validation of a chemical kinetic model. The experimental ignition delay time data are recorded using low- and high-pressure shock tubes and two rapid compression machines (RCM) to include all of the designed conditions. These novel experiments provide a direct validation of the chemical kinetic model, NUIGMech1.1, and its performance is characterized via statistical analysis, with the agreement between experiments and model being within ~ 26.4% over all of the conditions studied, which is comparable with a general absolute uncertainty of the applied facilities (~ 20%). Sensitivity and flux analyses allow for the key reactions controlling the ignition behavior of the blends to be identified. Subsequent analyses are performed to identify those reactions which are important for the pure fuel components and for the blended fuels, and synergistic/antagonistic blending effects are therefore identified over the wide range of conditions. The overall performance of NUIGMech1.1 and the correlations generated are in good agreement with the experimental data.

1. Introduction

According to the U.S. Energy Information Administration (EIA) report 2019 [1], it is projected that global energy consumption will increase by approximately 28% in 2050 compared to 2018 levels, with fossil fuels providing approximately 77% of the total energy demand. Liquid fuels, natural gas, and coal are the most important sources amongst all fossil fuels. Liquid fuels, such as gasoline, diesel, etc. are predicted to represent around 33% of energy consumption, with natural gas at close to 30%, coal near 18%, with the remaining 19% corresponding to nuclear, hydropower, and renewable sources [2].

The combustion of fossil fuels is the main sources of CO_2, SO_x, and NO_x emissions, among other pollutants. In this regard, natural gas is considered preferable to other fossil fuels including liquid fuels and coal as it is a cleaner energy source, having the highest hydrogen/carbon ratio among them. Widely used in the domestic, transportation, and industrial sectors, liquefied natural gas (LNG) is typically composed of methane (82–100%) but can contain substantial amounts of ethane, propane and butane, while

* Corresponding authors.
E-mail addresses: snehasish.panigrahy@nuigalway.ie (S. Panigrahy), henry.curran@nuigalway.ie (H.J. Curran).

https://doi.org/10.1016/j.combustflame.2021.02.009

Table 1
IDTs for C_2H_4, C_2H_6, C_3H_8, and binary blends from the literature.

Facility	Fuel	p_C / atm	T_C / K	Year	Reference
ST/RCM	C_2H_4	1 – 40	773 – 2200	1999 – 2020	[5, 8, 19-22]
ST/RCM	C_2H_6	1 – 40	830 – 1862	1971 – 2020	[5, 9, 23-25]
ST/RCM	C_3H_8	1 – 40	689 – 2615	1977 – 2013	[26-31]
ST/RCM	C_2H_4/C_2H_6	1 – 40	800 – 2000	2020	[6]

liquified petroleum gas (LPG) includes mainly propane, and butane. To reduce emissions, it is necessary to improve the efficiency of combustion systems for which a detailed understanding of the controlling chemistry is essential. The oxidation kinetics of small hydrocarbons plays an important role as the base of any mechanism for alternative fuels. For these reasons, the combustion community is interested in enhancing our understanding of the chemistry controlling the oxidation of hydrocarbons to increase the efficiency of engines and to reduce emissions of pollutants such as soot, NOx, UHCs (unburned hydrocarbons), and greenhouse gases in general. A hierarchical [3–6] (bottom-up) strategy has proven to be a good way to develop reliable chemical kinetic mechanisms and improve our understanding of the chemistry controlling pyrolysis and oxidation.

Combustion properties of fuels such as ignition delay time (IDT), speciation profiles, flame speed, among others become invaluable for the optimization of combustors. Relevant experiments and modeling studies for mono-fuels and some blends, such as ethylene, ethane, and propane, have been carried out with different methods and are available in the literature [7–14].

Dagaut et al. [15–17] studied species profiles consumed and produced during the oxidation ethylene, ethane, and propane in a jet-stirred reactor (JSR) using fuel mixtures diluted with nitrogen, at equivalence ratios (φ) of 0.1 – 4.0, at pressures ranging from 1 to 10 atm in the temperature range 800–1250 K. Their work showed the importance of small molecule sub-mechanisms including CO_2, CH_2O, CH_4, C_2H_2, C_2H_4, and C_3H_6 on the combustion of higher hydrocarbons.

Lowry et al. [18] measured laminar premixed flame speeds of pure methane, ethane, propane, and their binary blends with methane, at φ = 0.7 – 1.3, in a constant-volume cylindrical vessel, in the pressure range 1–10 atm, at room temperature (298 K). They highlighted the need to extensively study the synergistic effect of blends in comparison to pure fuels.

Baigmohammadi et al. [5,6] measured IDTs for pure ethylene, ethane, and propane, and binary alkane/alkene blends in a shock tube (ST) and in a rapid compression machine (RCM) at φ = 0.5–2.0, at pressures ranging from 20 to 40 atm in the temperature range of 800–2000 K. They showed that the synergistic effect on the reactivity of the mixture is important not only based on the fuel blends but in each variable considered during combustion such as pressure, temperature, dilution, etc. These previous studies [5,6,15–17] also used chemical kinetic mechanisms to predict the experimental data presented and identify the most relevant chemical reactions controlling the oxidation of these fuels.

Despite the large amount of data available for pure ethylene, ethane, and propane fuels, there are comparatively fewer studies of their blends, Table 1.

The current study aims to address the lack of data for mixtures by providing IDT data for binary C_2H_4/C_3H_8 and C_2H_6/C_3H_8 blends over a wide range of temperatures, pressures, equivalence ratios, and dilutions relevant to engine and gas turbine conditions. It also aims to validate a detailed chemical kinetic model using the novel experiments and literature data. We first provide a summary of the experimental conditions and approaches taken for this study, followed by details of the modeling work. The results and discussion section encompasses all of the comparisons of the model performance with the experimental data. Additionally, a comparison of the most important reactions for the pure fuels and their binary blends are presented to determine the kinetics controlling the reactivity of the blends.

2. Design of experiments and experimental approaches

All of the measured IDTs collected and presented in this study were obtained using two different shock tubes (ST) and two rapid compression machines (RCMs). For those experiments carried out at NUI Galway at pressures ranging from 1 to 40 bar and intermediate-to-high-temperatures (> 1000 K), low- (LPST) (p_C = 1 bar) and high-pressure ($p_C \geq$ 20 bar) shock tubes (HPSTs) were applied. The IDT experiments corresponding to the relatively high-pressure (20 $\leq p_C \leq$ 40 bar) and low-temperature (< 1000 K) regimes were taken using a twin-piston RCM. Some experiments at working pressures of 40 bar and greater were measured using a single-piston RCM at the Physico-Chemical Fundamentals of Combustion (PCFC)-RWTH [32,33] Aachen University to enhance the fidelity of the experimental IDTs. Details of these facilities and their operating characteristics are available in the literature [6,34,35].

For the IDT experiments performed at NUIG, ethane, ethylene, and propane gases with a purity of 99.95% were supplied by Air liquid UK. BOC Ireland provided all other gases with purities of 99.99% for oxygen, nitrogen, argon, and 99.96% for helium. At the PCFC-RWTH Aachen University, the alkane/alkene gases were supplied by Westfalen AG with a 99.95% purity. All other gases were supplied by Westfalen AG and Praxair with purities of oxygen $\geq$ 99.995%, nitrogen $\geq$ 99.95%, and argon $\geq$ 99.996%.

To stochastically distribute the experimental IDTs, the experimental conditions for this study were generated using the Taguchi [36] approach by applying an L_9 matrix based on four parameters of propane concentration, pressure, equivalence ratio, and dilution and also three different levels for each parameter studied. This approach has already been described by Baigmohammadi et al. [5,6].

For the mixture conditions studied, the propane concentration in the fuel blends varies from 10 to 50%, at pressures ranging from 10 to 135 bar, for φ of 0.5 – 2.0 and at dilutions of 75 – 90% (75% N_2 + 0–15% Ar). However, the ratio between the diluents were changed at low–temperature regime (RCM) depending on the desired compressed gas temperature. A synopsis of the designed conditions is presented in Figure 1 and Table 2.

In the current study, most of the measured IDTs in the HPST and RCMs [10,33,37–42] are defined as the time between the end of compression and the maximum gradient in pressure ($\frac{dp}{dt}$) behind the reflected shock. However, we define the ignition event as the maximum gradient in CH^* ($\frac{dCH^*}{dt}$) behind the reflected shock in the LPST measured by a photomultiplier and also when the test mixture is highly diluted in the HPST. The corresponding uncertainties involved in the measured IDTs are discussed by Baigmohammadi et al. [5,6]. Based on the analysis, the uncertainties in compressed mixture temperatures ($\sigma_{Tc,5}$) and measured IDTs change for every individual experimental point depending on the initial temperature, pressure, and/or mixture composition. In this regard, the average uncertainties of the compressed temperatures and the measured IDTs in NUIG-L/HPSTs are estimated to be approximately $\pm$ 10 K and $\pm$ 25%, respectively. However, the compressed temper-

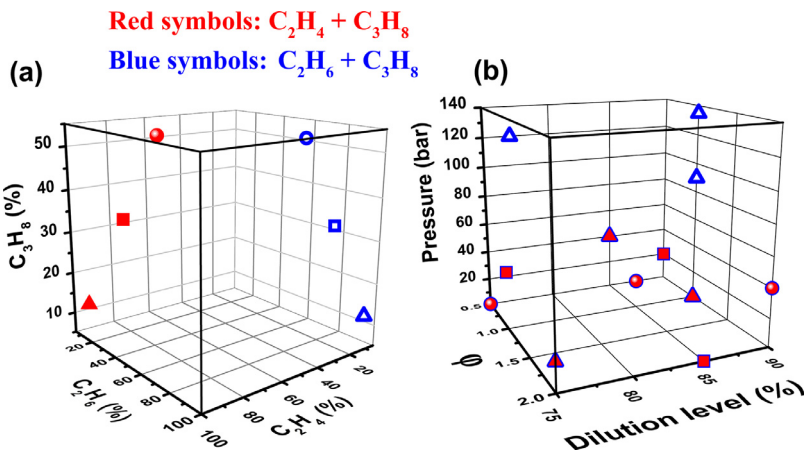

Fig. 1. Experimental Taguchi [36] L9 matrix of conditions. For 90%/10%, 70%/30%, and 50%/50% ratios (a) red: binary C_2H_4/C_3H_8 blends, blue: binary C_2H_6/C_3H_8 blends. (b) pressure, equivalence ratio, and dilution parameters. (For interpretation of the references to colour in this figure legend, the reader is referred to the web version of this article.)

Table 2
C_2H_4/C_3H_8 and C_2H_6/C_3H_8 mixture compositions in% mole volume in the current study. Where keywords NUIG refers to ST/RCM facilities at C^3-NUIGalway, and PCFC refers to RCM facility at PCFC-RWTH Aachen University, respectively.

	No.	% C_2H_6	% C_2H_4	% C_3H_8	% O_2	Dilution	φ	p_C / bar	Facility
C_2H_4/C_3H_8	1	0.000	1.40	1.400	22.20	75% N_2	0.5	1	NUIG
50%/50%	2	0.000	1.50	1.500	12.00	75% N_2+10% Ar	1.0	20	NUIG
	3	0.000	1.70	1.700	6.60	75% N_2+15% Ar	2.0	40	NUIG/ PCFC
C_2H_4/C_3H_8	4	0.000	3.75	1.610	9.64	75% N_2+10% Ar	2.0	1	NUIG
70%/30%	5	0.000	0.85	0.360	8.790	75% N_2+15% Ar	0.5	20	NUIG
	6	0.000	3.80	1.600	19.60	75% N_2	1.0	40	NUIG
C_2H_4/C_3H_8	7	0.000	2.10	0.200	7.70	75% N_2+15% Ar	1.0	1	NUIG
90%/10%	8	0.000	8.60	1.000	15.40	75% N_2	2.0	20	NUIG
	9	0.000	1.80	0.200	13.00	75% N_2+10% Ar	0.5	40	NUIG/ PCFC
C_2H_6/C_3H_8	10	1.300	0.00	1.300	22.40	75% N_2	0.5	1	NUIG
50%/50%	11	1.430	0.00	1.430	12.14	75% N_2+10% Ar	1.0	20	NUIG
	12	1.600	0.00	1.600	6.80	75% N_2+15% Ar	2.0	40	NUIG/ PCFC
C_2H_6/C_3H_8	13	3.530	0.00	1.510	9.96	75% N_2+10% Ar	2.0	1	NUIG
70%/30%	14	0.790	0.00	0.340	8.87	75% N_2+15% Ar	0.5	20	NUIG
	15	3.535	0.00	1.515	19.95	75% N_2	1.0	40	NUIG
C_2H_6/C_3H_8	16	1.940	0.00	0.220	7.84	75% N_2+15% Ar	1.0	1	NUIG
90%/10%	17	8.000	0.00	0.900	16.10	75% N_2	2.0	20	NUIG
	18	1.600	0.00	0.200	13.20	75% N_2+10% Ar	0.5	40	NUIG/ PCFC
	19	1.860	0.00	0.210	7.53	45.2% N_2+45.2% Ar	1.0	90	PCFC
	20	2.520	0.00	0.280	20.40	76.8% N_2	0.5	120	PCFC
	21	1.860	0.00	0.210	7.53	65.4% N_2+25% Ar	1.0	135	PCFC

ature uncertainty and the measured IDT variation in the NUIG and PCFC RCMs are evaluated to be about ± 5 – 15 K and ± 20% over the entire range of conditions.

3. Computational modeling

In the current study, NUIGMech1.1 is used to simulate the experimental targets. This mechanism comprises 2746 species and 11,270 reactions, which is developed based on series of recent experimental [4–6,43–47] and theoretical studies [48–50]. These works are outcome of continuous evolution of the detailed NUIGMech1.1 model which is extensively validated in the prior studies for oxidation of C_1– C_2 hydrocarbons [5,6], natural gas mixtures [44], propane/propene blends [47], propyne [45], iso-butene [51], as well as auto-ignition and pyrolysis of C_2 – C_6 alkenes [4,46]. The current work is a part of simultaneous development of the overall NUIGMecah1.1 mechanism. For the purpose of comparison, AramcoMech3.0 [52] is also utilized to perform simulations against the IDT experimental data from this study. Modifications of the most important reactions explicit to ethane, ethylene and propane chemistry in NUIGMech1.1 have not been mentioned in detail in previous publications [5,6,43,50], and thus are discussed in this study.

The experimental results were simulated using Python scripts based on the Cantera 2.4 [53] library and the CHEMKIN-Pro 18.2 [54] software. Cantera is suitable for automatization making data manipulation faster; however, Chemkin-Pro is faster for simulations involving large mechanisms and thus is more suitable for simulations when a full mechanism is required. As mentioned above, the definition of IDT is taken as the maximum gradient of pressure or radical concentration with respect to time for the ST simulations. In the RCM simulations, facility effects are included using the volume-time profiles derived from non-reactive experimental pressure-time traces in which O_2 is replaced by N_2 in the mixture [55,56].

The global model uncertainties, ϵMAD and ϵMAPE, are calculated based on the differences between the experimental data and mechanism simulated data using the Mean Absolute Deviations (MAD), and the Mean Absolute Percentage Error (MAPE), Eqs. (1) and (2), respectively. However, to analyze the data with an individual error, the Relative Percentage Error (RPE), εRPE, was used (Eq. (3)) to generate the histograms presented in this work. The

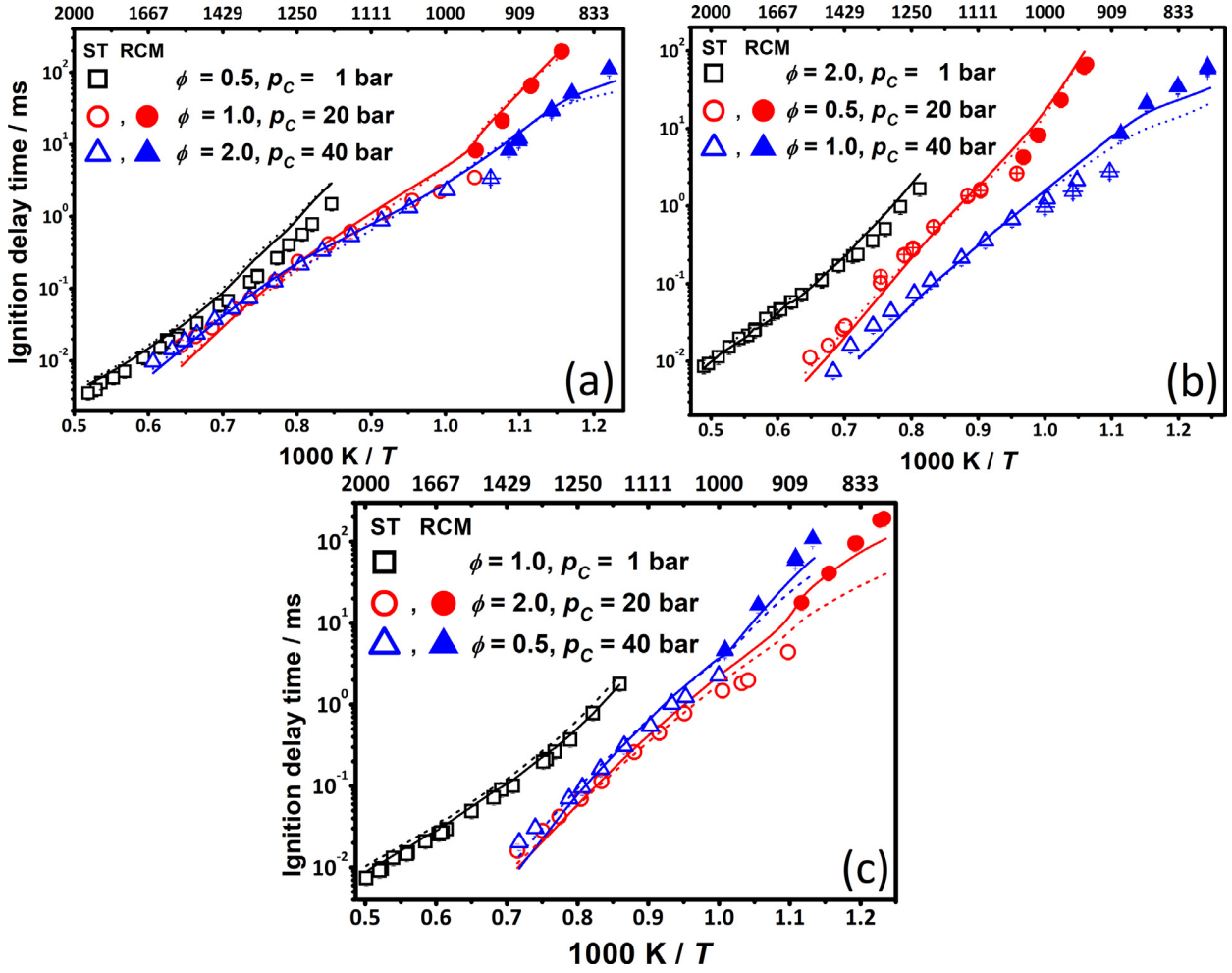

Fig. 2. Comparisons of experimental ST and RCM data against model predictions using NUIGMech1.1 (solid lines) and AramcoMech3.0 (dashed lines) for (a) a 50% C_2H_4/50% C_3H_8 blend at 75% N_2 (black symbols/lines), 75% N_2+10% Ar (red symbols/lines), and 75% N_2+15% Ar (blue symbols/lines), (b) a 70% C_2H_4/30% C_3H_8 blend at 75% N_2+10% Ar (black symbols/lines), 75% N_2+15% Ar (red symbols/lines), and 75% N_2 (blue symbols/lines), and (c) a 90% C_2H_4/10% C_3H_8 blend at 75% N_2+15% Ar (black symbols/lines), 75% N_2 (red symbols/lines), and 75% N_2+10% Ar (blue symbols/lines). (For interpretation of the references to colour in this figure legend, the reader is referred to the web version of this article.)

mathematical expressions used are the following:

$$\epsilon\mathrm{MAD} = \frac{1}{n}\sum^{|IDT\mathrm{mod}-IDT\mathrm{exp}|} \quad (1)$$

$$\epsilon\mathrm{MAPE} = \frac{1}{n}\sum^{\left(\left|\frac{IDT\mathrm{mod}-IDT\mathrm{exp}}{IDT\mathrm{exp}}\right|\right)} * 100 \quad (2)$$

$$\varepsilon\mathrm{RPE} = \left(\frac{IDT\mathrm{mod}-IDT\mathrm{exp}}{IDT\mathrm{exp}}\right) * 100 \quad (3)$$

where n is the total number of experimental measurements. Further details about the statistical analysis are provided as Supplementary material.

To identify the reactions controlling IDTs, brute-force sensitivity analyses were performed at the experimental conditions presented in this study. The sensitivity coefficient (S; [57]) is defined as:

$$S = \frac{In(\tau+/\tau-)}{In(k+/k-)} = \frac{In(\tau+/\tau-)}{In(2.0/0.5)}$$

The sensitivity coefficient S calculated using the brute force method is based on the IDT (τ), with the pre-exponential factor in the Arrhenius equations for each reaction perturbed in the sensitivity analysis. The sensitivity coefficient can be negative or positive, where a negative value refers to a reaction promoting reactivity (decreasing IDT), while a positive value refers to a reaction inhibiting reactivity (increasing IDT). Furthermore, rate of production (ROP) analyses were carried out to track the consumption of the blends and the production of intermediate species.

A global correlation discussion based on constant volume (CV) IDT simulations using NUIGMech1.1 is presented in the "Regression analysis" section (Section 4.5), together with general equations sorted by various temperature and pressure conditions. The aim of these correlations is to provide an easy and quick way to determine the IDT behavior of binary fuels. This does not require any kind of software pre-set up, and the coefficients of interest can be directly substituted in the equations provided in the respective section. A complete table of coefficient values and further details are provided as Supplementary material.

4. Results and discussions

All of the experimental results for the ethane/propane (C_2H_6/C_3H_8) and ethylene/propane (C_2H_4/C_3H_8) blends are presented in Section 4.1 together with simulations using NUIGMech1.1 and AramcoMech3.0 [52]. Henceforth, in all figures, the open symbols represent experimental LPST and/or HPST data, and the solid symbols represent the experimental low-temperature RCM data. Sections 4.2 – 4.4 present results for the effects of blend composition, pressure, and equivalence ratio using NUIGMech1.1 and their

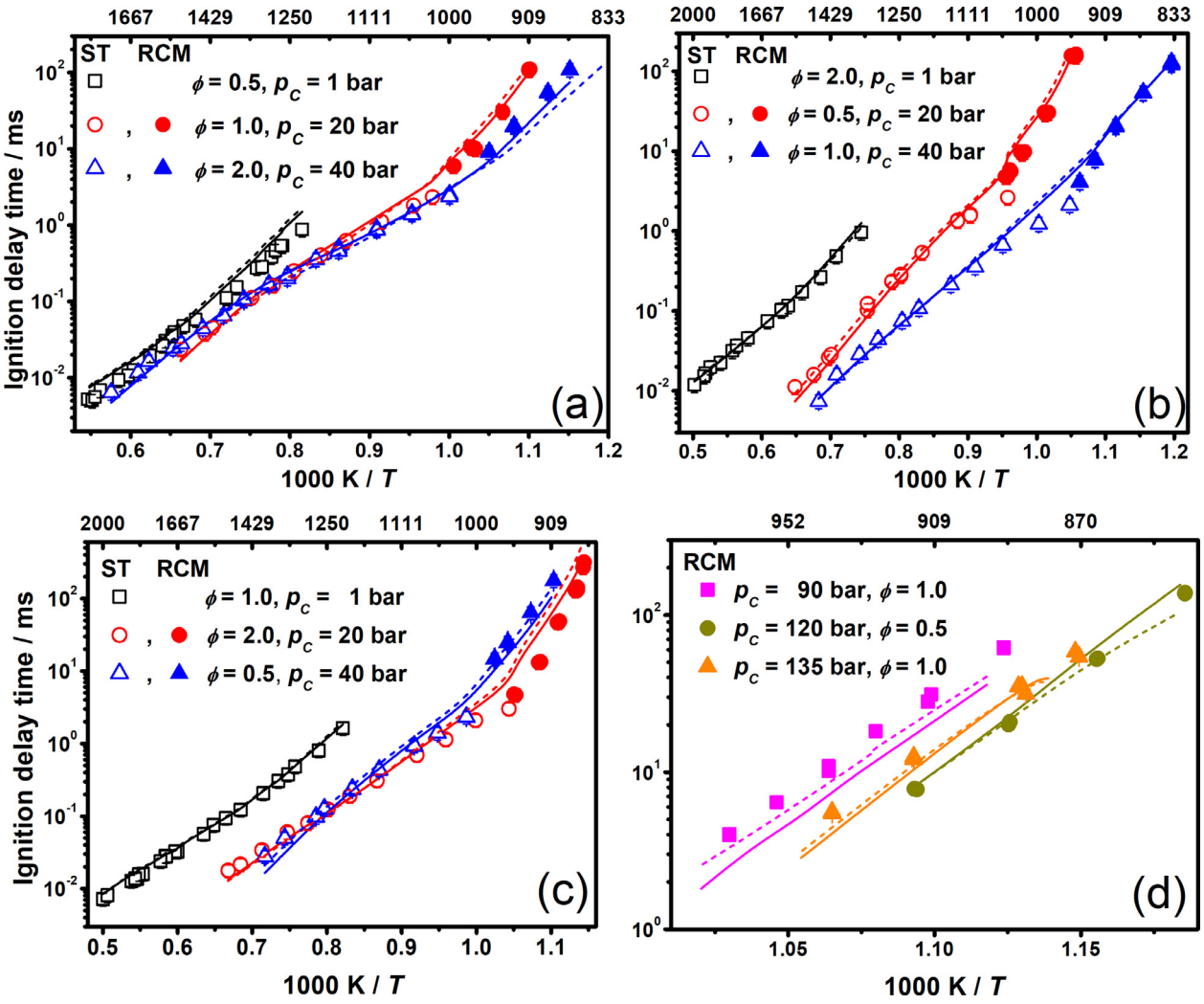

Fig. 3. Comparisons of experimental ST and RCM data against model predictions using NUIGMech1.1 (solid lines) and AramcoMech3.0 (dashed lines), for (a) a 50% C_2H_6/50% C_3H_8 blend at 75% N_2 (black symbols/lines), 75% N_2+10% Ar (red symbols/lines), and 75% N_2+15% Ar (blue symbols/lines), (b) a 70% C_2H_6/30% C_3H_8 blend at 75% N_2+10% Ar (black symbols/lines), 75% N_2+15% Ar (red symbols/lines), and 75% N_2 (blue symbols/lines), (c) a 90% C_2H_6/10% C_3H_8 blend at 75% N_2+15% Ar (black symbols/lines), 75% N_2 (red symbols/lines), and 75% N_2+10% Ar (blue symbols/lines) and (d) a 90% C_2H_6/10% C_3H_8 blend at 45.2% N_2+45.2% Ar (magenta symbols/lines), 76.8% N_2 (green symbols/lines), and 65.4% N_2+25% Ar (orange symbols/lines). (For interpretation of the references to colour in this figure legend, the reader is referred to the web version of this article.)

corresponding correlations. Finally, Section 4.5 discusses the correlation performance.

4.1. Ethylene/propane and ethane/propane blends

Figures 2 and 3 present experimental data and model predictions of IDTs over the range of conditions studied for the binary C_2H_4/C_3H_8 and C_2H_6/C_3H_8 blends. Figures 2 and 3 show that NUIGMech1.1 is in better agreement than AramcoMech3.0 with the experimental data. Statistical analyses were conducted using the IDTs from the experiments, and those calculated using both NUIGMech1.1 and AramcoMech3.0. A total sample of 328 IDTs was used to determine the mean, standard deviation (σ), mean absolute deviation (MAD), relative percentage error (RPE), and mean absolute percentage error (MAPE). Figure S10(a) and S10(b), with "S" notation referring to the Supplementary material, provide the RPE frequency distribution for NUIGMech1.1 and AramcoMech3.0 relative to the IDT experiments. It can be inferred that the differences between NUIGMech1.1 and AramcoMech3.0 are a consequence of the poor predictions of AramcoMech3.0 in the low-temperature regime for the C_2H_4/C_3H_8 blends. Furthermore, the absolute value of MAPE calculated over the entire dataset using NUIGMech1.1 was 26.4%, while that for AramcoMech3.0 is 31.9%, indicating the greater accuracy of NUIGMech1.1. As it can accurately predict the IDT data measured over a wide range of temperatures, pressures and equivalence ratios, CV simulations are performed using NUIGMech1.1 to understand the effects of these operating conditions on the IDTs of the pure fuels and their binary blends.

4.2. Synergistic/antagonistic effect of blends

First, the ignition behavior of the pure fuels is analyzed to determine the important reactions controlling the reactivity. In Fig. 4, the IDT predictions for C_2H_4/air, C_2H_6/air, and C_3H_8/air mixtures at fuel-lean conditions, at p_C = 40 bar and T_C in the range 740 – 1660 K are shown. At lower temperatures (T_C < 1050 K), C_3H_8 is the fastest fuel to ignite, however, the trend reverses at higher temperatures, and propane is the slowest to react compared to both C_2H_4 and C_2H_6. The reactivity of C_2H_4 is observed to be higher than C_2H_6 at all temperatures studied here.

To explore the controlling chemistry at high-temperature conditions, ROP analyses for C_2H_4/air, C_2H_6/air, and C_3H_8/air mixtures

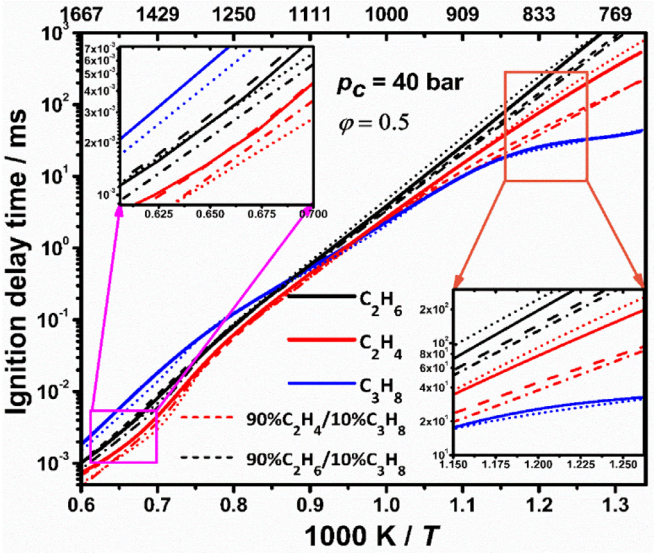

Fig. 4. IDT predictions of pure fuels, 90% C_2H_4/10% C_3H_8 and 90% C_2H_6/10% C_3H_8 binary blend in air. The corresponding derived correlation predictions are marked as dotted lines for pure fuels and dotted-dashed for binary blends.

are illustrated in Fig. 5 at T_C = 1430 K and p_C = 40 bar. The ROP analyses are performed following an elemental carbon (C) balance. The percentage value above the arrow refers to the percentage of the fuel proceeding through that pathway. The reaction paths represent the promoting (red color) and inhibiting (blue color) channels of the corresponding fuels. At high temperatures, the reactivity of all fuels is governed by the dominating chain branching reaction $\dot{H} + O_2 \leftrightarrow \ddot{O} + \dot{O}H$, which depends on the concentrations of $\dot{H}$ atoms and O_2. In the case of C_2H_4/air ignition, at 1430 K, the fuel mainly undergoes H-atom abstraction by $\dot{O}H$ and $\dot{H}$ producing vinyl ($\dot{C}_2H_3$) radicals. This radical reacts with O_2 to generate vinoxy radical ($\dot{C}H_2CHO$) through the chain branching reaction $\dot{C}_2H_3 + O_2 \leftrightarrow \dot{C}H_2CHO + \ddot{O}$. Oxygen atoms further react with ethylene greatly promoting reactivity by generating $\dot{H}$ atoms through two different channels, $C_2H_4 + \ddot{O} \leftrightarrow \dot{C}H_2CHO + \dot{H}$ (18.1%) and $C_2H_4 + \ddot{O} \leftrightarrow \dot{C}H_2 + CH_2O$ (16%) followed by $\dot{C}H_2 + O_2 \leftrightarrow CO_2 + \dot{H} + \dot{H}$. For the reaction of oxygen atoms with ethylene the total rate constant and the branching fractions through the various product channels ($\dot{C}H_3 + H\dot{C}O$, $\dot{C}H_2CHO + \dot{H}$, $\dot{C}H_2 + CH_2O$, $CH_2CO + H_2$) are taken from the calculations by Li et al. [58]. These are in good agreement available experimental data, as shown in Fig. 6(a). Figure 6(b) compares the rate constants for the individual pathways associated with the $C_2H_4 + \ddot{O}$ system. AramcoMech3.0 used the rate constants for $C_2H_4 + \ddot{O}$ producing $\dot{C}H_3 + H\dot{C}O$ and $\dot{C}H_2CHO + \dot{H}$ based on the Baulch et al. [59] recommendation. The pathway producing $\dot{C}H_2 + CH_2O$ was not included in AramcoMech3.0, and its inclusion in NUIGMech1.1 significantly increases the predicted reactivity. The effect of updating the rate constant for the $C_2H_4 + \ddot{O} \rightarrow$ products reactions on IDT predictions for C_2H_4/air mixtures is shown in Fig. S19 of the Supplementary material. The $\dot{C}H_2CHO$ radical formed here further decomposes to produce ketene and $\dot{H}$ atom, Fig. 5(a). The formation of substantial concentrations of $\dot{H}$ atoms is responsible for the faster ignition of C_2H_4/air mixtures at higher temperatures.

Ethylene is an important intermediate formed during C_2H_6 oxidation. At 1430 K, C_2H_6 consumption is initiated by H-atom abstraction primarily by $\dot{O}H$ and $\dot{H}$ forming ethyl ($\dot{C}_2H_5$) radicals. There has been a wide variety of experimental investigations for these rate constants, as shown in Fig. S13. NUIGMech1.1 has an updated rate constant for H-atom abstraction by $\dot{O}H$ based on the fit recommended by Krasnoperov and Michael [69]. For H-atom abstraction by $\dot{H}$ atoms, we have adopted the theoretical calculations from Sivaramakrishnan et al. [70]. $\dot{C}_2H_5$ radicals decompose promptly to C_2H_4 and $\dot{H}$ atoms, which undergo chain branching by reacting with O_2 via $\dot{H} + O_2 \leftrightarrow \ddot{O} + \dot{O}H$, promoting reactivity. However, at 1430 K, approximately 15% of $\dot{C}_2H_5$ radicals react with O_2 to form C_2H_4 via H-atom abstraction that competes

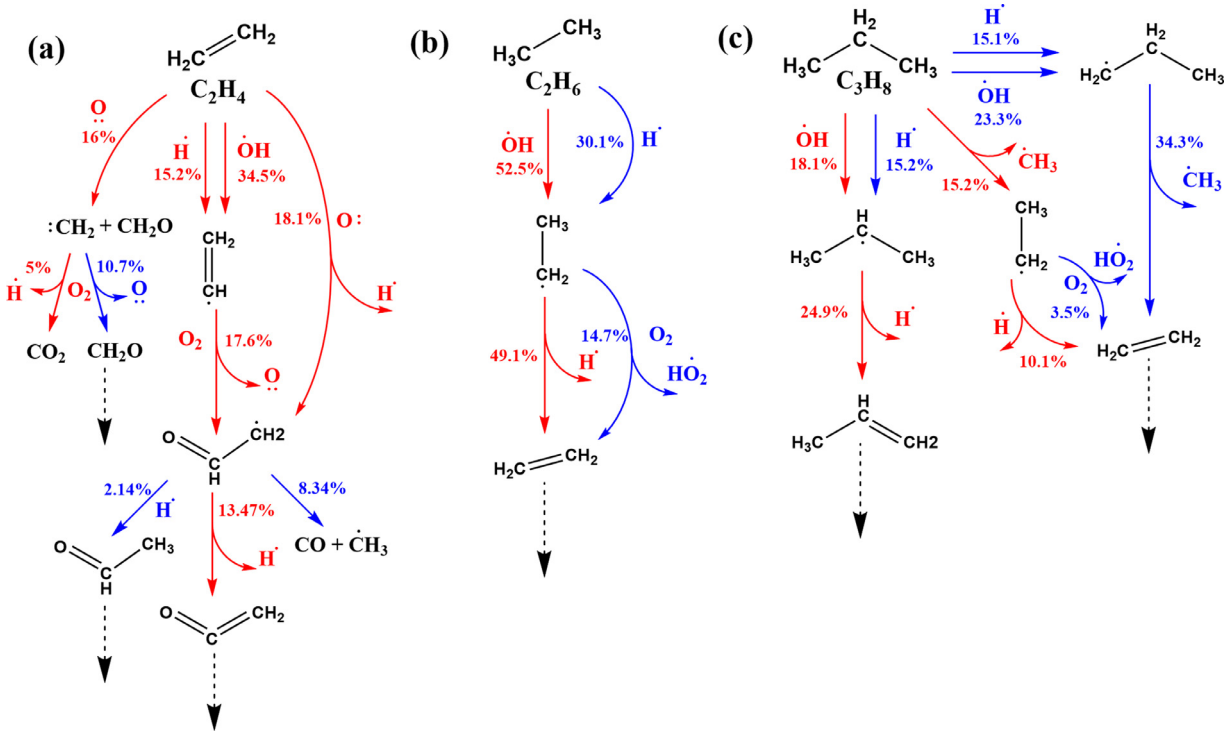

Fig. 5. Flux analyses of pure (a) C_2H_4, (b) C_2H_6, and (c) C_3H_8 fuel ignition for T_C = 1430 K, p_C = 40 bar and φ = 0.5, at the time of 15% fuel consumption.

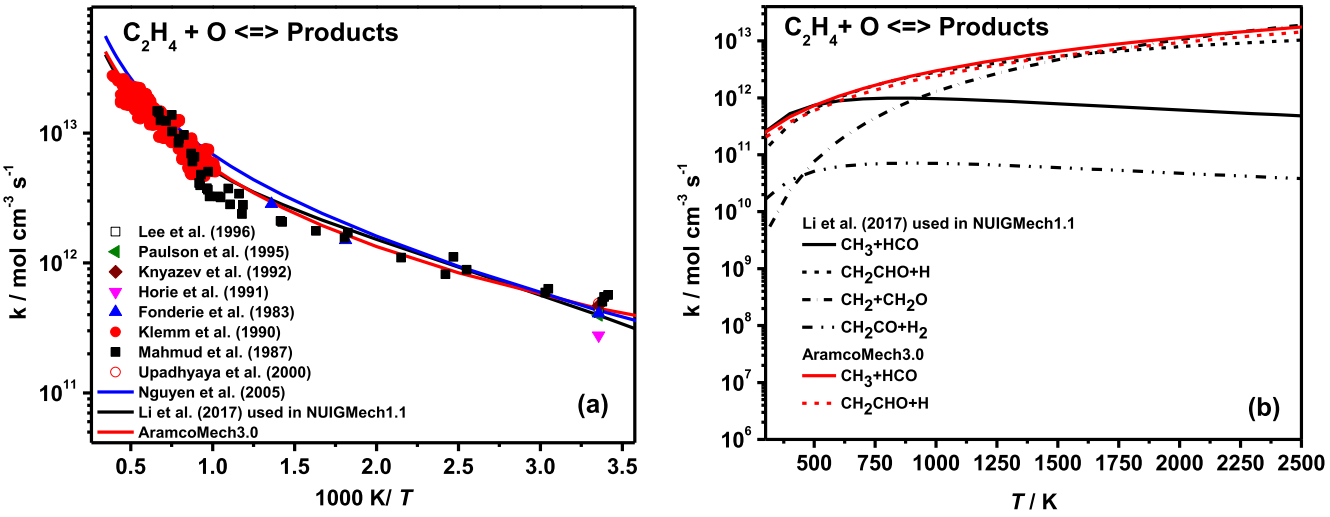

Fig. 6. Comparisons for experimental and theoretical determinations for (a) the total reaction rate constant of C_2H_4 + Ö [58, 60-68] and (b) product pathways for the reaction C_2H_4 + Ö.

with $\dot{C}_2H_5$ radical decomposition. The subsequent reaction pathways associated with the C_2H_6 consumption flux are governed by the high-temperature chemistry of C_2H_4, as discussed in the previous paragraph. At higher temperature conditions, $\dot{C}_2H_5 + O_2 \leftrightarrow C_2H_4 + H\dot{O}_2$, as well as the H-atom abstraction by Ḣ from the fuel which competes with the major chain branching reaction $\dot{H} + O_2 \leftrightarrow \ddot{O} + \dot{O}H$, are responsible for the lower reactivity of C_2H_6 compared to C_2H_4.

Similar to ethane and ethylene, propane oxidation is mainly driven by H-atom abstraction by ȮH radicals and Ḣ atoms, generating primary ($n\dot{C}_3H_7$) and secondary propyl ($i\dot{C}_3H_7$) radicals. Due to the importance of H-atom abstraction by ȮH from propane, there have been a large number of measurements performed, Fig. S14. The rate constants adopted in this work are best fits from the more recent direct measurements by Sivaramakrishnan et al. [71], who investigated the branching fraction for the abstraction of the secondary C–H bond in the temperature range 927 – 1146 K, together with the measurement by Droege and Tully [72] over the temperature range 298–900 K (Fig. S14). At 1430 K, approximately 15% of the C_3H_8 is consumed by unimolecular decomposition producing $\dot{C}_2H_5$ and methyl ($\dot{C}H_3$) radicals, Fig. 5(c). Substantial concentrations of $\dot{C}H_3$ radicals are also formed from the β-scission of $n\dot{C}_3H_7$ radicals. Methyl radicals are consumed by reaction with $H\dot{O}_2$ to produce methoxy radicals through the chain branching reaction $\dot{C}H_3 + H\dot{O}_2 \leftrightarrow \dot{C}H_3O + \dot{O}H$, which promotes reactivity. The route through the chain-terminating reaction $\dot{C}H_3 + H\dot{O}_2 \leftrightarrow CH_4 + O_2$ inhibits reactivity. This competition between chain branching and termination significantly influences IDT predictions for C_3H_8. The rate constants for these reactions are taken from the theoretical calculations of Jasper et al. [73] and Zhu and Lin [74] respectively. The rate constants and the branching ratio of the two $\dot{C}H_3 + H\dot{O}_2$ channels agree well with the most recent experimental measurements by Hong et al. [75] (Fig. S15). The self-recombination of $\dot{C}H_3$ radicals producing C_2H_6 further contributes to a reduction in the reactivity of propane. The presence of high concentrations of $\dot{C}H_3$ radicals ultimately decreases the reactivity of C_3H_8 compared to C_2H_6 at high-temperature conditions.

The effects on IDTs of the addition of C_3H_8 to C_2H_4/air and C_2H_6/air mixtures are presented in Fig. 4. The reactivities of the mixtures increase significantly for the 90% C_2H_4/10% C_3H_8 and 90% C_2H_6/10% C_3H_8 binary blends at lower temperatures in the range 740–1000 K. The addition of only 10% C_3H_8 to the C_2H_4/air and C_2H_6/air mixtures shortens IDTs by a factor of 2.8 and 2.0 respectively, at 790 K. To interpret the influence of C_3H_8 addition on the ignition of the C_2H_4/air and C_2H_6/air mixtures, sensitivity analyses were performed at 790 K, Fig. 7. Moreover, Figure 8 illustrates the flux analyses performed for these mixtures in the same condition. The black color represents the flux for the pure C_2H_4/air or C_2H_6/air mixtures, and the red color represents the flux for the C_3H_8 blended binary mixtures. The flux analysis presented in Fig. 8 shows that adding propane to the mixture does not alter the reaction pathways of ethylene and ethane chemistry nor does it significantly affect their flux values.

At 790 K, for both pure C_2H_4 and the 90% C_2H_4/10% C_3H_8 blend, ethylene is primarily consumed by the addition of ȮH radical to the double bond forming hydroxyethyl radicals, which accounts for approximately 70% of the overall C_2H_4 consumption. These radicals add to molecular oxygen producing hydroxyethyl-peroxy radicals ($\dot{O}_2C_2H_4OH$), which subsequently decompose, producing two formaldehyde molecules and an ȮH radical or form vinyl alcohol and $H\dot{O}_2$ radicals, the former being the most favorable product channel promoting reactivity for the C_2H_4/air mixture, Fig. 8(a). Besides ȮH addition, $H\dot{O}_2$ addition to ethylene producing oxirane (C_2H_4O1–2) and an ȮH radical and this reaction also has a large promoting effect on the reactivity of ethylene at low temperatures, especially for fuel-rich conditions.

The importance of the $C_2H_4 + H\dot{O}_2 \leftrightarrow C_2H_4O1\text{–}2 + \dot{O}H$ and $\dot{O}_2C_2H_4OH \rightarrow$ products reaction systems on C_2H_4 oxidation is shown in Fig. 9(a), which also presents the performance of the current mechanism and AramcoMech3.0 as can be seen by the red solid lines and black dashed lines, respectively for the 90% C_2H_6/10% C_3H_8 mixtures at p_C = 20 atm, and φ = 2.0. AramcoMech3.0 severely under-predicts the IDTs, particularly in the low temperature region in the range 800–900 K. AramcoMech3.0 implemented a reaction rate for $C_2H_4 + H\dot{O}_2 \leftrightarrow C_2H_4O1\text{–}2 + \dot{O}H$ based on the recommendation by Zsély et al. [11]. Recently Zádor et al. [77] and Klippenstein [76] studied the potential energy surfaces of the $C_2H_5\dot{O}_2$ system using high-level quantum chemistry calculations. NUIGMech1.1 has adopted the rate constant for $C_2H_4 + H\dot{O}_2$ from Klippenstein [76], which is approximately a factor of three lower than the rate constant recommended by Zsély et al. [11] at 800 K, Fig. 9(b). Updating this rate constant in AramocMech3.0 leads to a significant improvement in IDT predictions as depicted by the dashed-dotted line in Fig. 9(a). Another important reaction pathway controlling ethylene IDT is the consumption of $\dot{O}_2C_2H_4OH$ radicals through the Waddington

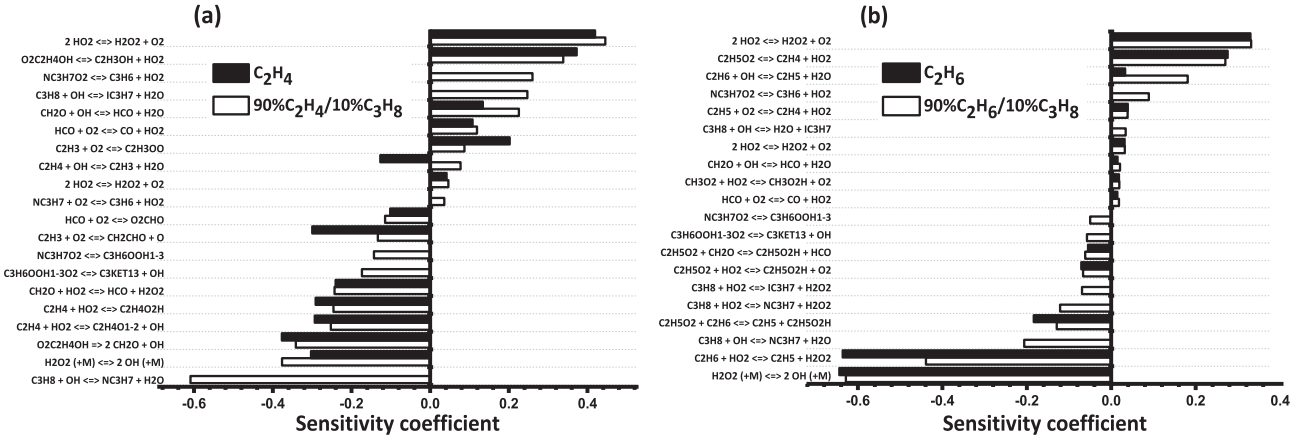

Fig. 7. Sensitivity analyses to IDT at 790 K, $p_C = 40$ atm, $\varphi = 0.5$, for (a) C_2H_4 and 90% C_2H_4/10% C_3H_8, in air, and (b) C_2H_6 and 90% C_2H_6/10% C_3H_8 in air.

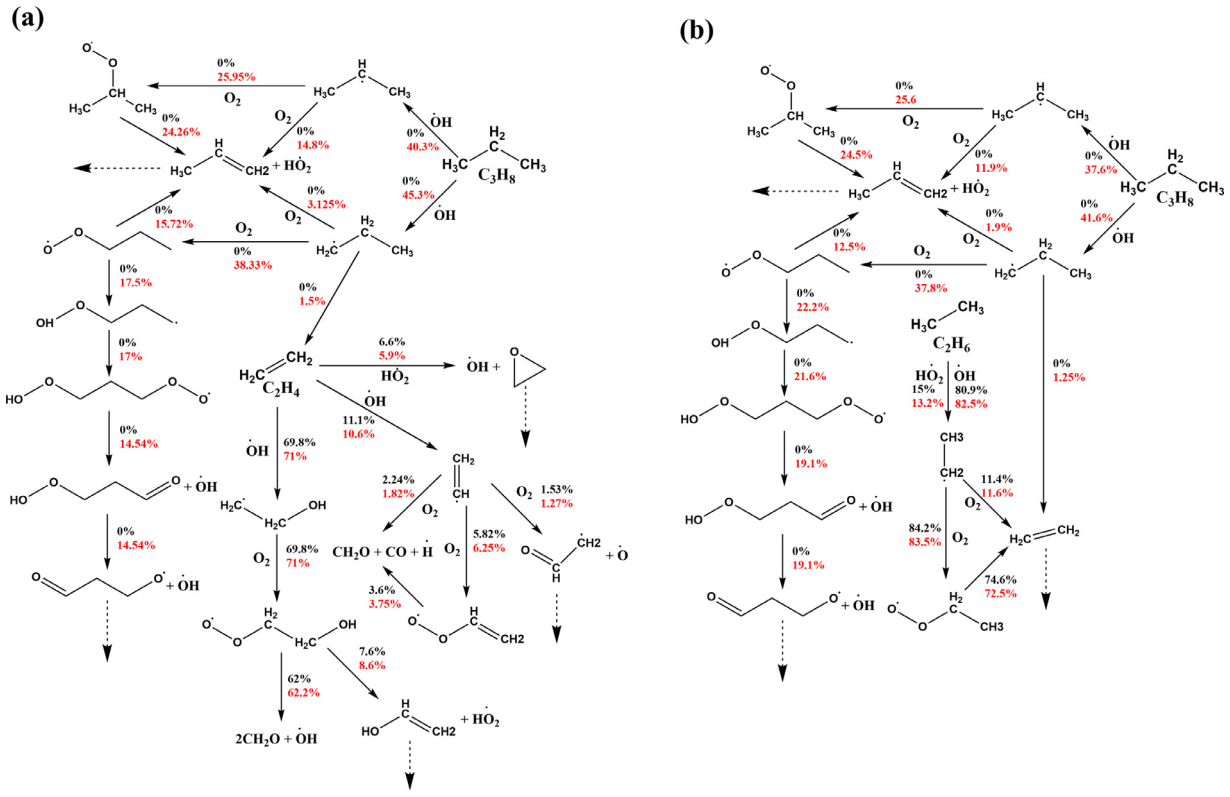

Fig. 8. Flux analyses for (a) pure C_2H_4 (black) and 90% C_2H_4/10% C_3H_8 (red), (b) pure C_2H_6 (black) and 90% C_2H_6/10% C_3H_8 (red) mixtures ignition for 790 K and at $p_C = 40$ atm, and $\varphi = 0.5$. (For interpretation of the references to colour in this figure legend, the reader is referred to the web version of this article.)

[79] mechanism $\dot{O}_2C_2H_4OH \rightarrow 2CH_2O + \dot{O}H$ and the $H\dot{O}_2$ elimination channel producing C_2H_3OH which inhibits reactivity. In NUIG-Mech1.1 the rate constant for the dissociation of $\dot{O}_2C_2H_4OH$ radicals is adopted from Zádor et al. [78]. AramcoMech3.0 utilized an estimated rate constant for the Waddington pathway that is an order of magnitude higher than the rate determined by Zádor et al. [78], while surprisingly, the $H\dot{O}_2$ elimination channel was not included in the mechanism. The last agreement represented by the solid black line in Fig. 9(a) is attained by updating both C_2H_4+$H\dot{O}_2$ and dissociations of $\dot{O}_2C_2H_4OH$ reactions in AramcoMech3.0 that leads to significant improvement in the agreement of the simulations compared to the experimental measurements.

As seen in Fig. 8(a), $\dot{O}H$ radicals can abstract hydrogen atoms from ethylene producing $\dot{C}_2H_3$ radicals. These add to O_2 generating vinyl-peroxy radicals, which subsequently dissociate to formaldehyde, CO, and $\dot{H}$ atoms. Some $\dot{C}_2H_3$ radicals also produce $\dot{C}H_2CHO$ and $\ddot{O}$ atoms increasing the reactivity of ethylene ignition, as shown in Fig. 8(a). For the C_2H_6/air mixture, the fuel is mainly consumed by H-atom abstraction by $\dot{O}H$ and $H\dot{O}_2$ radicals forming $\dot{C}_2H_5$ radicals. These react with O_2 to produce ethylperoxy ($C_2H_5\dot{O}_2$) radicals, which subsequently decompose to C_2H_4 and $H\dot{O}_2$ radicals. Figure 7(b) shows that the concerted elimination reaction $C_2H_5\dot{O}_2 \leftrightarrow C_2H_4 + H\dot{O}_2$ is important in inhibiting the autoignition of C_2H_6.

Figure 7(a) and 7(b) shows that C_3H_8 specific reactions become important when propane is added to the C_2H_4/air and C_2H_6/air mixtures. At 790 K, H-atom abstraction from C_3H_8 by $\dot{O}H$ producing $n\dot{C}_3H_7$ and H_2O is the most sensitive reaction promoting reactivity, while abstraction leading to $i\dot{C}_3H_7$ radicals inhibits reactivity. At 790 K, ~14.8% (C_2H_4/C_3H_8 blend) and ~11.9% (C_2H_6/C_3H_8

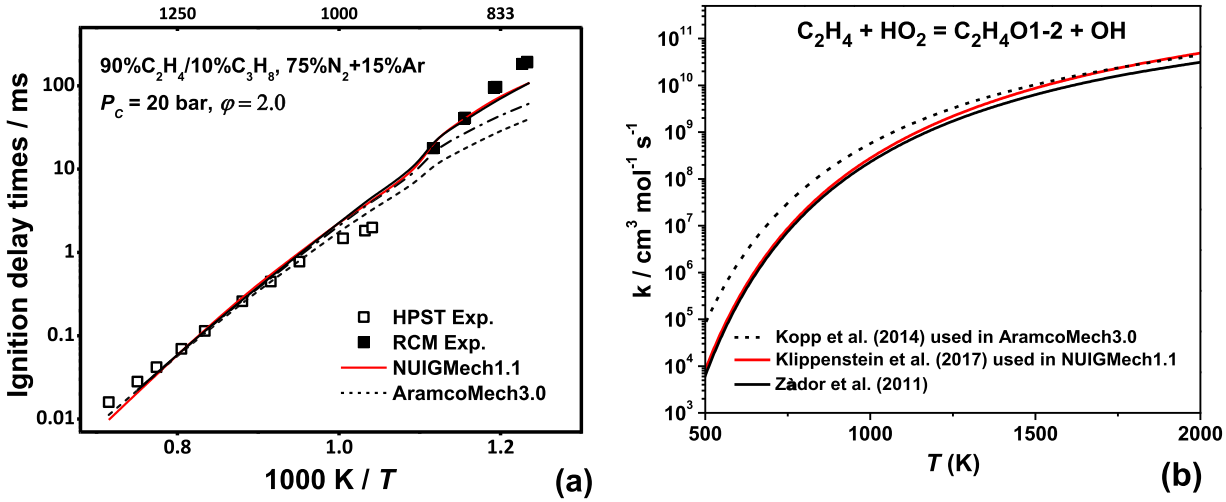

Fig. 9. (a) Effect of changing the rate constant for $C_2H_4 + H\dot{O}_2 \leftrightarrow C_2H_4O1\text{–}2 + \dot{O}H$ and $\dot{O}_2C_2H_4OH \rightarrow$ products on IDT predictions for 90%C_2H_4/10%C_3H_8 mixtures, — NUIGMech1.1, ------ AramcoMech3.0, –□–□ AramcoMech3.0 plus updated rate constant [76] for $C_2H_4 + H\dot{O}_2 \leftrightarrow C_2H_4O1\text{–}2 + \dot{O}H$, — AramcoMech3.0 plus updated rate constant for $C_2H_4 + H\dot{O}_2 \leftrightarrow C_2H_4O1\text{–}2 + \dot{O}H$ and $\dot{O}_2C_2H_4OH \rightarrow$ products [77]. (b) Comparison of current rate constant [75] for $C_2H_4 + H\dot{O}_2 \leftrightarrow C_2H_4O1\text{–}2 + \dot{O}H$ against the study by Zsély et al. [11] and Zádor et al. [78].

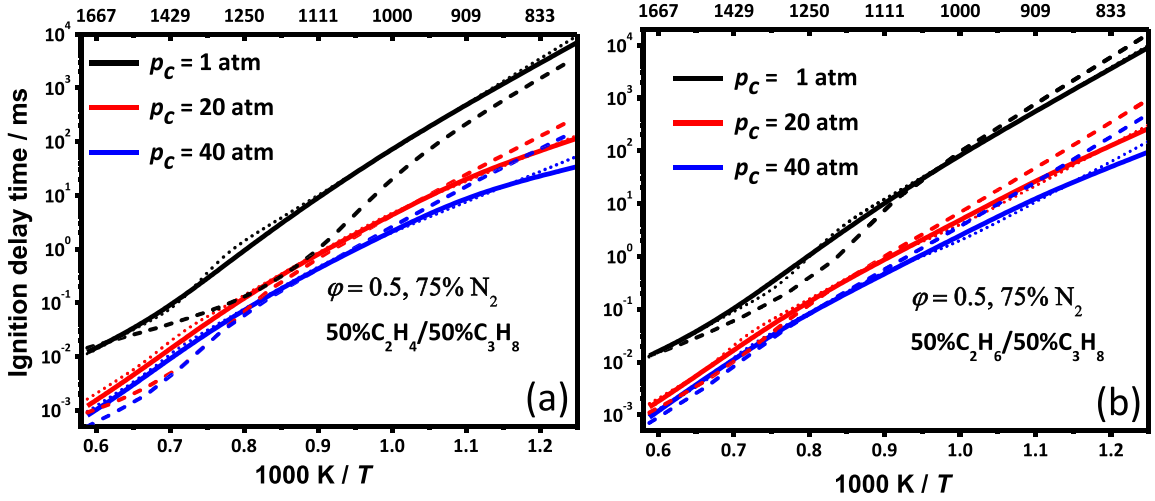

Fig. 10. Effect of pressure for (a) 50% C_2H_4/50% C_3H_8 (solid lines) binary blend and pure ethylene (dashed lines), (b) 50% C_2H_6/50% C_3H_8 (solid lines) binary blend and pure ethane (dashed lines). The derived correlation predictions for binary blends are represented by dotted lines.

blend) of $i\dot{C}_3H_7$ radicals react with O_2 to form C_3H_6 and $H\dot{O}_2$ radicals, which reduces reactivity. However, ~38.3% (C_2H_4/C_3H_8 blend) and ~37.8% (C_2H_6/C_3H_8 blend) of $n\dot{C}_3H_7$ radicals add to O_2 forming n-propyl-peroxy ($n\dot{C}_3H_7O_2$) radicals which undergo isomerization generating hydroperoxyl-propyl ($\dot{C}_3H_6OOH1\text{–}3$) radicals. These then further add to O_2 producing hydroperoxyl-propyl peroxy radicals ($\dot{C}_3H_6OOH1\text{–}3O_2$), which isomerize to produce carbonylhydroperoxides and $\dot{O}H$ radicals. The carbonylhydroperoxide can further dissociate, producing a carbonyl-alkoxy radical and a second $\dot{O}H$ radical, which is a chain branching pathway, resulting in higher reactivity of the C_3H_8 blended mixtures compared to the pure C_2H_4/air or C_2H_6/air mixtures.

4.3. Effect of pressure on ignition

Figure 10 presents the influence of pressure on the IDTs for the 50% C_2H_4/50% C_3H_8 and 50% C_2H_6/50% C_3H_8 binary blended mixtures as well as for pure C_2H_4 and C_2H_6 at φ = 0.5 and 75% N_2 dilution. The model predicts that the reduction in reactivity due to the addition of C_3H_8 with C_2H_4 at 1 atm is more than for the corresponding 20 atm and 40 atm cases at intermediate and higher temperature conditions. The self-recombination of methyl radicals is responsible for the lower reactivity of the propane blended mixtures as discussed in Section 4.2. In the case of the C_2H_4/C_3H_8 blend at 1250 K, as the pressure decreases to 1 atm the $\dot{C}H_3 + \dot{C}H_3$ (+M) $\leftrightarrow C_2H_6$ (+M) reaction more strongly inhibits reactivity, accounting for 35% of the total flux through methyl radicals, while at 40 bar this reaction contributes only 12% to $\dot{C}H_3$ consumption. Furthermore, from Fig. 10 it is observed that the overall reactivity of the system increases with pressure due to the corresponding increase in the concentration of the reactants. At 800 K, upon increasing the pressure from 1 to 20 atm, there is an order of magnitude increase in reactivity observed for both the C_2H_4/C_3H_8 and C_2H_6/C_3H_8 mixtures. There is approximately a four-fold increase in reactivity by increasing the pressure from 20 to 40 atm. To determine the reactions controlling IDT predictions at these conditions, sensitivity analyses are presented in Fig. 11 and Fig. S16 for the binary mixtures at p_C = 1, 20, and 40 atm.

Figure 11 shows that at low temperature (800 K) and high-pressure conditions (20 and 40 atm), the reactivity of the binary blends is mainly controlled by H-atom abstraction from C_3H_8 by $\dot{O}H$ radicals, with the formation of $n\dot{C}_3H_7$ radicals promoting reac-

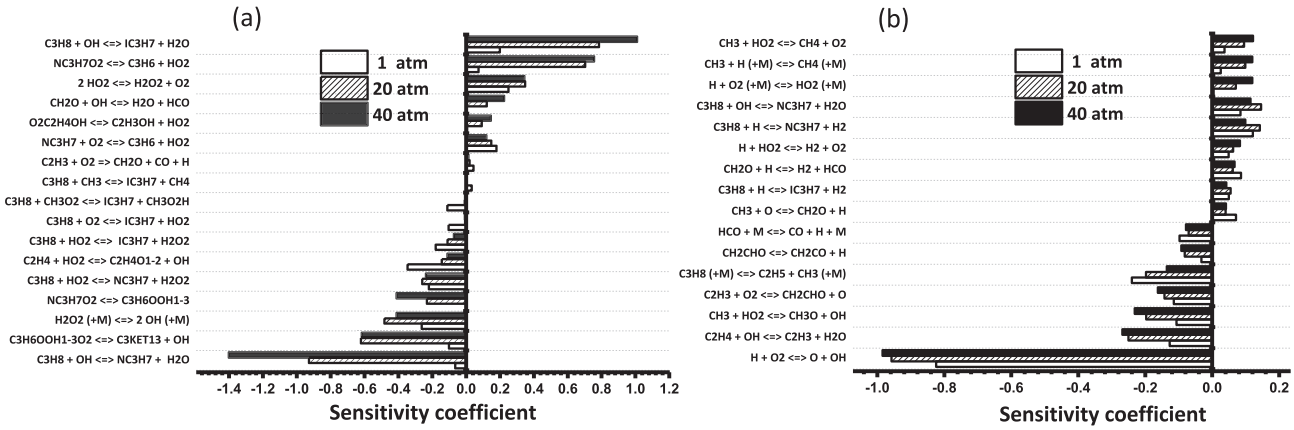

Fig. 11. Sensitivity analyses to IDT predictions as function of pressure at $\varphi = 0.5$, 50% C_2H_4/50% C_3H_8. (a) 800 K and (b) 1600 K.

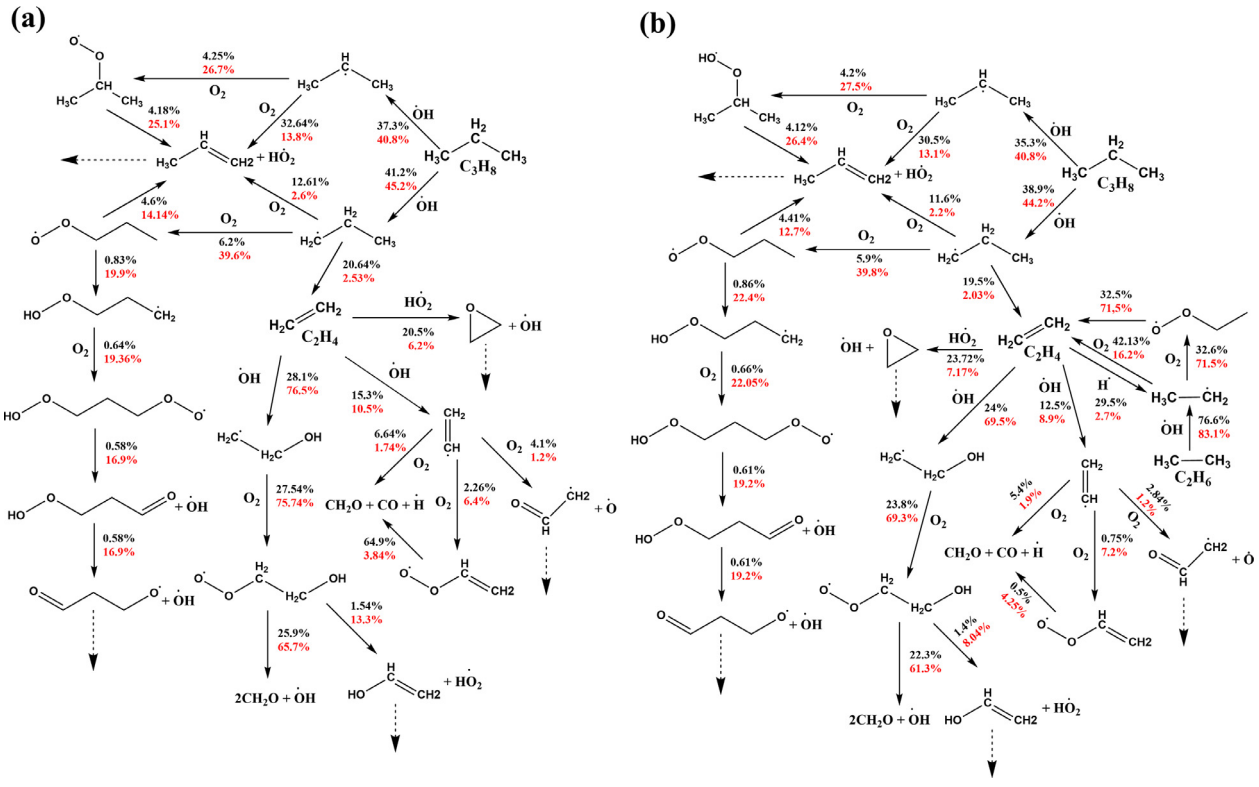

Fig. 12. Flux analyses at 800 K, $\varphi = 0.5$, $p = 1$ (black), and 40 atm (red), with 75% N_2 as diluent for (a) 50% C_2H_4/50% C_3H_8, and (b) 50% C_2H_6/50% C_3H_8. (For interpretation of the references to colour in this figure legend, the reader is referred to the web version of this article.)

tivity and $i\dot{C}_3H_7$ radicals inhibiting reactivity. However, at 800 K and 1 atm, H-atom abstraction from C_3H_8 no longer influences IDT predictions, but rather the competition between the reactions generating and consuming hydrogen peroxide, via $H\dot{O}_2 + H\dot{O}_2 \leftrightarrow H_2O_2 + O_2$ and H_2O_2 (+M) $\leftrightarrow \dot{O}H + \dot{O}H$ (+M), respectively control the reactivity of the binary blends. The flux analyses presented in Figure 12 show that, at 40 atm pressure, the percentage contribution of $n\dot{C}_3H_7$ radical β-scission forming C_2H_4 and $\dot{C}H_3$ reduces, while the importance of $n\dot{C}_3H_7$ radical addition to O_2 increases compared to the 1 atm case. Since the addition of $n\dot{C}_3H_7$ radicals to O_2 and the subsequent chain branching channels produces two reactive $\dot{O}H$ radicals and thus increases reactivity, the formation of $n\dot{C}_3H_7$ radicals, and other low-temperature reactions those are not favorable at low pressures become significant in controlling the overall reactivity of the binary mixtures at higher pressures . At the higher temperature of 1600 K, the reactivity is only controlled by the chain branching reaction, $\dot{H} + O_2 \leftrightarrow \ddot{O} + \dot{O}H$ irrespective of pressure, as seen in Figs. 11(b) and S16. The reactions that consume $\dot{H}$ atoms such as, $C_3H_8 + \dot{H} \leftrightarrow n\dot{C}_3H_7 + H_2$, $C_3H_8 + \dot{H} \leftrightarrow i\dot{C}_3H_7 + H_2$, $C_2H_6 + \dot{H} \leftrightarrow \dot{C}_2H_5 + H_2$, $CH_2O + \dot{H} \leftrightarrow H\dot{C}O + H_2$ and $\dot{H} + O_2$ (+M) $\leftrightarrow H\dot{O}_2$ (+M) compete with $\dot{H} + O_2 \leftrightarrow \ddot{O} + \dot{O}H$ and thus inhibit the reactivity of the binary mixtures (Fig. 11).

4.4. Effect of equivalence ratio on ignition

Figure 13 presents the effect of equivalence ratio on IDTs for the pure fuels, 50% C_2H_4/50% C_3H_8 and 50% C_2H_6/50% C_3H_8 binary mixtures at $p_C = 20$ atm, 75% N_2, and at $\varphi = 0.5$, 1.0, and 2.0. It is observed that at temperatures above 1250 K, the reactivities of both the pure fuels and the binary mixtures are fastest for the fuel-lean mixtures and slowest for the fuel-rich mixtures. However, at a temperature below 1250 K, fuel-rich mixtures are fastest to ignite, and the fuel-lean mixtures are slowest. To determine the governing chemistry under these conditions, sensitivity analyses were per-

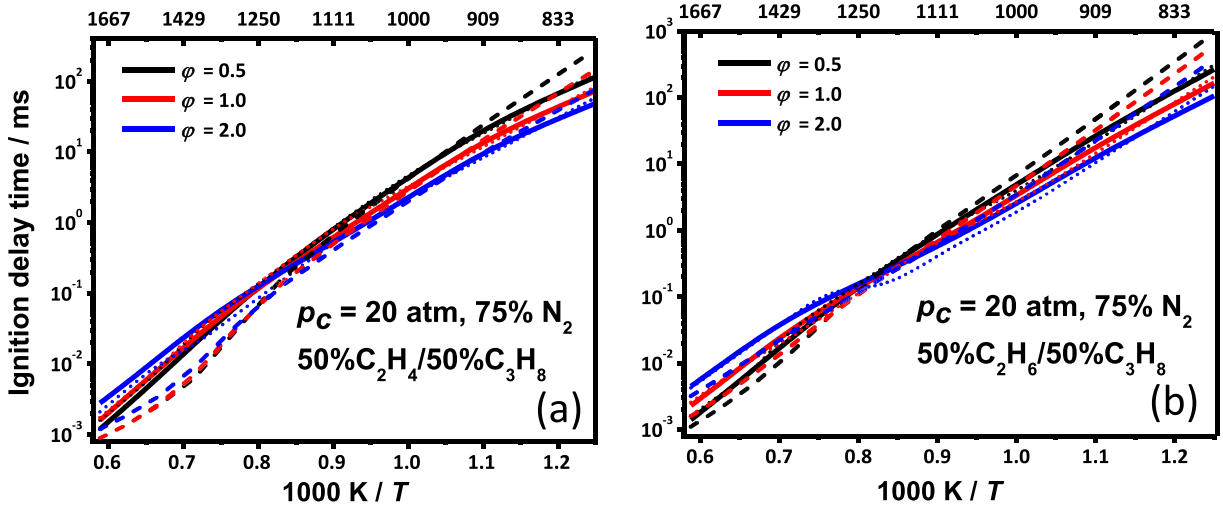

Fig. 13. Effect of equivalence ratio in (a) 50% C_2H_4/50% C_3H_8 (solid lines) binary blend and pure ethylene (dashed lines), (b) 50% C_2H_6/50% C_3H_8 (solid lines) binary blend and pure ethane (dashed lines). The derived correlation predictions for binary blends are represented by dotted lines.

formed, the results of which are presented as a function of equivalence ratio in Figs. S17 and S18 at 800 K and 1600 K. At high temperatures (> 1250 K), IDTs are mainly controlled by the concentration of O_2 in the binary blends through the main chain branching reaction $\dot{H} + O_2 \leftrightarrow \ddot{O} + \dot{O}H$, and its influence increases as the mixture become leaner. Thus, fuel-lean mixtures are fastest to ignite at high temperatures. However, at low temperatures (< 1250 K), the reactivity is mainly governed by the addition of the fuel derived alkyl radicals to O_2 and the following low-temperature chemistry leading to chain branching, which is limited by the fuel concentration through H-atom abstraction from propane by $\dot{O}H$ radicals. Thus, at a lower temperature, the dependence on the equivalence ratio is reversed, with fuel-rich mixtures being the most reactive.

4.5. Regression analysis

Global regression equations have been developed using NUIG-Mech1.1 with approximately 17,280 CV simulations for each blend mixture spanning over five parameters: p_C (1 – 40 atm), T_C (800 – 2000 K), φ (0.2 – 2.0), dilution (75% – 90%) and fuel ratio composition (50% C_2H_4 or C_2H_6/50% C_3H_8, and 70% C_2H_4 or C_2H_6/30% C_3H_8). The regression equations developed using the predictions are compared with the ST experimental data in Fig. S20 and S21 of the Supplementary material. The expression (τ_{corr}) used is analogous to the Arrhenius rate expression and is defined as shown in Eq. (4) below:

$$\tau corr = 10^{A} e^{\frac{B}{T_C}} [C_2H_4]^{C} [C_2H_6]^{D} [C_3H_8]^{E} [oxidizer]^{F} [diluent]^{G} \quad (4)$$

where A represents the pre-exponential factor coefficient, B represents the activation energy, and C – G are the concentration dependencies of ethylene, ethane, propane, oxidizer, and dilution, respectively. A synopsis of the derived correlations for the binary fuels studied in the pressure range $20 \le p_C \le 40$ atm over three regimes of temperature is presented below. However, details of the coefficients of the derived correlations along with their corresponding χ^2 and R^2 for the C_2H_4/C_3H_8 and C_2H_6/C_3H_8 mixtures are presented in Table S6 and S7, respectively.

For $1500 \le T_C \le 2000$ K:

$$\tau corr = 10^{-10.34} e^{\frac{21,386.6}{T_C}} [C_2H_4]^{-0.502} [C_3H_8]^{0.463} [oxidizer]^{-1.080} [diluent]^{0.354} \quad (5)$$

$$\tau corr = 10^{-9.402} e^{\frac{204.65}{T_C}} [C_2H_6]^{0.113} [C_3H_8]^{0.413} [oxidizer]^{-1.344} [diluent]^{0.131} \quad (6)$$

For $1100 \le T_C \le 1500$ K:

$$\tau corr = 10^{-9.89} e^{\frac{192.20.37}{T_C}} [C_2H_4]^{-0.491} [C_3H_8]^{-0.056} [oxidizer]^{-0.447} [diluent]^{0.149} \quad (7)$$

$$\tau corr = 10^{-9.79} e^{\frac{190.65.65}{T_C}} [C_2H_6]^{-0.408} [C_3H_8]^{-0.169} [oxidizer]^{-0.330} [diluent]^{0.062} \quad (8)$$

For $800 \le T_C \le 1100$ K:

$$\tau corr = 10^{-7.217} e^{\frac{14.136.9}{T_C}} [C_2H_4]^{-0.44} [C_3H_8]^{-0.392} [oxidizer]^{-0.427} [diluent]^{-0.017} \quad (9)$$

$$\tau corr = 10^{-9.52} e^{\frac{18.630.7}{T_C}} [C_2H_6]^{-0.145} [C_3H_8]^{-0.555} [oxidizer]^{-0.186} [diluent]^{-0.145} \quad (10)$$

At high temperatures (1500–2000 K), the coefficient for ethylene is strongly negative, while those for ethane and propane are positive. This is because at high temperatures increasing the ethylene concentration increases the concentration of vinyl radicals, which react with O_2 ($\dot{C}_2H_3 + O_2 \leftrightarrow \dot{C}H_2CHO + \ddot{O}$) in a reaction which is chain branching. On the other hand, both ethane and propane compete with O_2 for $\dot{H}$ atoms, and if their concentrations increase, the rate of $\dot{H} + O_2 \leftrightarrow \ddot{O} + \dot{O}H$ decreases, reducing reactivity. For ethane/propane mixtures, both coefficients are positive, but it is less positive for ethane than for propane, as the oxidation of ethane leads to higher concentrations of ethylene. Thus, increasing the concentration of ethane relative to propane will increase reactivity and vice versa.

At low temperatures (800–1100 K), the coefficients associated with ethylene, ethane, and propane become negative, with ethane being less negative than propane. At low temperatures, propane promotes reactivity through the addition of *n*-propyl radicals to

O_2 that proceeds to chain branching through the low-temperature reaction sequence that generates two highly active $\dot{O}H$ radicals. Thus, for the ethane/propane mixtures, increasing the propane concentration will increase mixture reactivity. However, for ethylene/propane mixtures, the coefficient of ethylene is comparable to that of propane, as ethylene and propane exhibit similar reactivities in the temperature range between 900 and 1100 K, as seen in Fig. 4.

It is interesting to note that, at high temperatures Eqs. (5) and ((6)), the magnitude of the oxidizer coefficients (–1.08 and –1.344 for C_2H_4/C_3H_8 and C_2H_6/C_3H_8 blends, respectively) are significantly larger, by a factor of two or more, than for the corresponding fuel coefficients, thus showing a higher sensitivity towards oxidizer concentrations at these conditions. As we approach the lower temperature regimes Eqs. (9) and ((10)), the coefficients associated with each fuel become higher and are even larger than the corresponding oxidizer coefficients, thus representing the increasing importance of fuel-based kinetics. These characteristics observed in the correlations corroborate the discussion of the underlying kinetics in Section 4 above and enable the correlations to capture the IDT trends effectively.

5. Conclusions

An experimental and kinetic modeling study of the IDT characteristics of C_2 – C_3 binary blends of C_2H_4/C_3H_8 and C_2H_6/C_3H_8 mixtures over a wide range of experimental conditions, pressures (1–135 atm), temperatures (~750–2000 K), equivalence ratios ($0.5 \leq \varphi \leq 2.0$) and 75–90% of dilution percentage were presented. The performance of NUIGMech1.1 and its corresponding derived correlations were evaluated against the experimental data collected. Results show that NUIGMech1.1 is in good agreement within ~26.4% of model uncertainty to the measured IDTs over the studied conditions, compared to ~35% for AramcoMech3.0. Moreover, correlations can predict the experimental IDTs appropriately under specific regimes, becoming a useful tool in predicting the behavior of C_2 – C_3 binary blends at specific conditions.

Finally, the effects of blend composition, pressure and equivalence ratio on IDTs were investigated for various mixtures containing C_2H_4, C_2H_6, and C_3H_8 as reactants. It was observed that for all mixtures, as the temperature and pressure increase, IDTs decrease. For the effect of equivalence ratio, an expected crossover point was observed at T_C ~ 1250 K, wherein the controlling chemistry switches such that the trends invert their behavior. The reactivity of C_2H_4 was found to be higher than for C_2H_6 throughout the temperature range examined in this study. At higher temperatures, vinoxy radicals and oxygen atoms formed from the reaction of vinyl radicals with O_2, proceed via dissociation and bimolecular reactions with C_2H_4, to produce a substantial amount of $\dot{H}$ atoms resulting in faster ignition of C_2H_4/air mixtures. The concerted elimination reaction between $\dot{C}_2H_5$ and O_2 is responsible for the reduction in ethane reactivity. It was observed that C_3H_8 blended fuels were the fastest to ignite at lower temperatures (< 1250 K), however, the trend is reversed at higher temperatures, and C_3H_8 exhibited the slowest reactivity compared to both C_2H_4 and C_2H_6 at $T >$ 1250 K. In the case of C_3H_8, at low temperatures *n*-propyl radical formation, followed the classical low-temperature chain branching pathways via its addition to O_2 generate $\dot{O}H$ radicals promoting reactivity, while methyl radical recombination and reaction with $H\dot{O}_2$ leading to CH_4 and O_2 reduces reactivity at higher temperatures.

Declaration of Competing Interest

The authors declare that they have no known competing financial interests or personal relationships that could have appeared to influence the work reported in this paper.

Acknowledgments

The authors would like to express their gratitude to Science Foundation Ireland (SFI) via their Research Centre Program through project numbers 15/IA/3177 and 16/SP/3829, KAY-ICHEC via the project ngche079c, and to Shell Research Ltd. The authors from PCFC RWTH Aachen University would like to recognize the funding support from the German Research Foundation (Deutsche Forschungsgemeinschaft, DFG) through the project number –322460823 (HE7599/2–1).

Supplementary materials

Supplementary material associated with this article can be found, in the online version, at doi:10.1016/j.combustflame.2021.02.009.

References

[1] U.S.E.I. Administration, International energy outlook 2019 with projections to 2050, IEO2019, 2019.
[2] S. Bilgen, Structure and environmental impact of global energy consumption, Renew. Sustain. Energy Rev. 38 (2014) 890–902.
[3] W.K. Metcalfe, S.M. Burke, S.S. Ahmed, H.J. Curran, A hierarchical and comparative kinetic modeling study of C1−C2 hydrocarbon and oxygenated fuels, Int. J. Chem. Kinet. 45 (2013) 638–675.
[4] S.S. Nagaraja, J. Liang, S. Dong, S. Panigrahy, A. Sahu, G. Kukkadapu, S.W. Wagnon, W.J. Pitz, H.J. Curran, A hierarchical single-pulse shock tube pyrolysis study of C2–C6 1-alkenes, Combust. Flame 219 (2020) 456–466.
[5] M. Baigmohammadi, V. Patel, S. Martinez, S. Panigrahy, A. Ramalingam, U. Burke, K.P. Somers, K.A. Heufer, A. Pekalski, H.J. Curran, A comprehensive experimental and simulation study of ignition delay time characteristics of single fuel C1−C2 hydrocarbons over a wide range of temperatures, pressures, equivalence ratios, and dilutions, Energy Fuels 34 (3) (2020) 3755–3771.
[6] M. Baigmohammadi, V. Patel, S. Nagaraja, A. Ramalingam, S. Martinez, S. Panigrahy, A.A.E. Mohamed, K.P. Somers, U. Burke, K.A. Heufer, A. Pekalski, H.J. Curran, Comprehensive experimental and simulation study of the ignition delay time characteristics of binary blended methane, ethane, and ethylene over a wide range of temperature, pressure, equivalence ratio, and dilution, Energy Fuels 34 (7) (2020) 8808–8823.
[7] M.M. Kopp, N.S. Donato, E.L. Petersen, W.K. Metcalfe, S.M. Burke, H.J. Curran, Oxidation of ethylene–air mixtures at elevated pressures, part 1: experimental results, J. Propuls. Power 30 (2014) 790–798.
[8] M.M. Kopp, E.L. Petersen, W.K. Metcalfe, S.M. Burke, H.J. Curran, Oxidation of ethylene-air mixtures at elevated pressures, part 2: chemical kinetics, J. Propuls. Power 30 (2014) 799–811.
[9] C.J. Aul, W.K. Metcalfe, S.M. Burke, H.J. Curran, E.L. Petersen, Ignition and kinetic modeling of methane and ethane fuel blends with oxygen: a design of experiments approach, Combust. Flame 160 (2013) 1153–1167.
[10] S.M. Gallagher, H.J. Curran, W.K. Metcalfe, D. Healy, J.M. Simmie, G. Bourque, A rapid compression machine study of the oxidation of propane in the negative temperature coefficient regime, Combust. Flame 153 (2008) 316–333.
[11] I.G. Zsély, T. Nagy, J.M. Simmie, H.J. Curran, Reduction of a detailed kinetic model for the ignition of methane/propane mixtures at gas turbine conditions using simulation error minimization methods, Combust. Flame 158 (2011) 1469–1479.
[12] A. Burcat, R.W. Crossley, K. Scheller, Shock tube investigation of ignition in ethane-oxygen-argon mixtures, Symp. (Int.) Combust. 18 (1972) 115–123.
[13] H. Hashemi, J.G. Jacobsen, C.T. Rasmussen, J.M. Christensen, P. Glarborg, S. Gersen, M. van Essen, H.B. Levinsky, S.J. Klippenstein, High-pressure oxidation of ethane, Combust. Flame 182 (2017) 150–166.
[14] S. Gersen, A.V. Mokhov, J.H. Darmeveil, H.B. Levinsky, P. Glarborg, Ignition-promoting effect of NO_2 on methane, ethane and methane/ethane mixtures in a rapid compression machine, Proc. Combust. Inst. 33 (2011) 433–440.
[15] P. Dagaut, J.C.C. Boettner, M. Cathonnet, Ethylene pyrolysis and oxidation: a kinetic modeling study, Int. J. Chem. Kinet. 22 (1990) 641–664.
[16] P. Dagaut, M. Cathonnet, J.C. Boettner, F. Gaillard, Kinetic modeling of propane oxidation, Combust. Sci. Technol. 56 (1987) 23–63.
[17] P. Dagaut, M. Cathonnet, J.c.c. Boettner, Kinetics of ethane oxidation, Int. J. Chem. Kinet. 23 (1991) 437–455.
[18] W. Lowry, J. de Vries, M. Krejci, E. Petersen, Z. Serinyel, W. Metcalfe, H. Curran, G. Bourque, Laminar flame speed measurements and modeling of pure alkanes and alkane blends at elevated pressures, Proceedings of ASME Turbo Expo 2010: Power for Land, Sea and Air (2010).
[19] C.J. Brown, G.O. Thomas, Experimental studies of shock-induced ignition and transition to detonation in ethylene and propane mixtures, Symp. (Int.) Combust. 117 (1999) 861–870 1999.

[20] D. Davidson, W. Ren, R. Hanson, Experimental database for development of a HiFiRE JP-7 surrogate fuel mechanism, Proceedings of the 50th AIAA Aerospace Sciences Meeting including the New Horizons Forum and Aerospace Exposition (2012).
[21] O.G. Penyazkov, K.L. Sevrouk, V. Tangirala, N. Joshi, High-pressure ethylene oxidation behind reflected shock waves, Proc. Combust. Inst. 32 (2009) 2421–2428.
[22] S. Saxena, M.S.P. Kahandawala, S.S. Sidhu, A shock tube study of ignition delay in the combustion of ethylene, Combust. Flame 158 (2011) 1019–1031.
[23] K.S. Alexander Burcat, A. Lifshitz, Shock-tube investigation of comparative ignition delay times for C1-C5 alkanes, Symp. (Int.) Combust. 16 (1971) 29–33 1971.
[24] J. de Vries, J.M. Hall, S.L. Simmons, M.J.A. Rickard, D.M. Kalitan, E.L. Petersen, Ethane ignition and oxidation behind reflected shock waves, Combust. Flame 150 (2007) 137–150.
[25] Y. Hidaka, K. Sato, H. Hoshikawa, T. Nishimori, R. Takahashi, H. Tanaka, K. Inami, N. Ito, Shock-tube and modeling study of ethane pyrolysis and oxidation, Combust. Flame 120 (2000) 245–264 2000.
[26] A.G. McLain, C.J. Jachimowski, Chemical kinetic modeling of propane oxidation behind shock waves, National Aeronautics and Space Administration, 1977.
[27] P. Cadman, G.O. Thomas, P. Butler, The auto-ignition of propane at intermediate temperatures and high pressures, Phys. Chem. Chem. Phys. 2 (2000) 5411–5419.
[28] Z. Qin, V.V. Lissianski, H. Yang, W.C. Gardiner, S.G. Davis, H. Wang, Combustion chemistry of propane: a case study of detailed reaction mechanism optimization, Proc. Combust. Inst. 28 (2000) 1663–1669.
[29] K.G. Yeong, S.G. Su, Shock tube and modeling study of the ignition of propane, Bull. Korean Chem. Soc. 22 (2001) 2001vol. 2022, no. 2003.
[30] J. Herzler, L. Jerig, P. Roth, Shock-tube study of the ignition of propane at intermediate temperatures and high pressures, Combust. Sci. Technol. 176 (2004) 1627–1637.
[31] E. Hu, Z. Zhang, L. Pan, J. Zhang, Z. Huang, Experimental and modeling study on ignition delay times of dimethyl ether/propane/oxygen/argon mixtures at 20bar, Energy Fuels 27 (2013) 4007–4013.
[32] C. Lee, S. Vranckx, K.A. Heufer, S.V. Khomik, Y. Uygun, H. Olivier, On the chemical kinetics of ethanol oxidation: shock tube, rapid compression machine and detailed modeling study, Z. Phys. Chem. 226 (1) (2012) 1–28.
[33] A. Ramalingam, K. Zhang, A. Dhongde, L. Virnich, H. Sankhla, H. Curran, A. Heufer, An RCM experimental and modeling study on CH_4 and CH_4/C_2H_6 oxidation at pressures up to 160bar, Fuel 206 (2017) 325–333.
[34] L. Brett, J. Macnamara, P. Musch, J.M. Simmie, Brief Communication: simulation of methane autoignition in a rapid compression machine with creviced pistons, Combust. Flame 124 (2001) 326–329.
[35] E.L. Petersen, M. Röhrig, D.F. Davidson, R.K. Hanson, C.T. Bowman, High-pressure methane oxidation behind reflected shock waves, Symp. (Int.) Combust. 26 (1996) 799–806.
[36] P.J. Ross, Taguchi techniques for quality engineering, McGraw-Hill Professional, New York, 1988.
[37] S.M. Burke, U. Burke, R. Mc Donagh, O. Mathieu, I. Osorio, C. Keesee, A. Morones, E.L. Petersen, W. Wang, T.A. DeVerter, M.A. Oehlschlaeger, B. Rhodes, R.K. Hanson, D.F. Davidson, B.W. Weber, C.J. Sung, J. Santner, Y. Ju, F.M. Haas, F.L. Dryer, E.N. Volkov, E.J.K. Nilsson, A.A. Konnov, M. Alrefae, F. Khaled, A. Farooq, P. Dirrenberger, P.A. Glaude, F. Battin-Leclerc, H.J. Curran, An experimental and modeling study of propene oxidation. Part 2: ignition delay time and flame speed measurements, Combust. Flame 162 (2015) 296–314.
[38] S.M. Burke, W. Metcalfe, O. Herbinet, F. Battin-Leclerc, F.M. Haas, J. Santner, F.L. Dryer, H.J. Curran, An experimental and modeling study of propene oxidation. Part 1: speciation measurements in jet-stirred and flow reactors, Combust. Flame 161 (2014) 2765–2784.
[39] U. Burke, K.P. Somers, P. O'Toole, C.M. Zinner, N. Marquet, G. Bourque, E.L. Petersen, W.K. Metcalfe, Z. Serinyel, H.J. Curran, An ignition delay and kinetic modeling study of methane, dimethyl ether, and their mixtures at high pressures, Combust. Flame 162 (2015) 315–330.
[40] D. Healy, H.J. Curran, S. Dooley, J.M. Simmie, D.M. Kalitan, E.L. Petersen, G. Bourque, Methane/propane mixture oxidation at high pressures and at high, intermediate and low temperatures, Combust. Flame 155 (2008) 451–461.
[41] D. Healy, H.J. Curran, J.M. Simmie, D.M. Kalitan, C.M. Zinner, A.B. Barrett, E.L. Petersen, G. Bourque, Methane/ethane/propane mixture oxidation at high pressures and at high, intermediate and low temperatures, Combust. Flame 155 (2008) 441–448.
[42] D. Healy, D.M. Kalitan, C.J. Aul, E.L. Petersen, G. Bourque, H.J. Curran, Oxidation of C1−C5 alkane quinternary natural gas mixtures at high pressures, Energy Fuels 24 (2010) 1521–1528.
[43] A. Mohamed, S. Panigrahy, A. Sahu, G. Bourque, H.J. Curran, An experimental and modeling study of the auto-ignition of natural gas blends containing C1–C7 n-alkanes, Proc. Combust. Inst. 38 (2021).
[44] S. Nagaraja, J. Power, G. Kukkadapu, S. Dong, S..W. Wangon, W.J. Pitz, H.J. Curran, A single pulse shock tube study of pentene isomer pyrolysis, Proc. Combust. Inst. 38 (2021).
[45] S. Panigrahy, J. Liang, S. Nagaraja, Z. Zuo, G. Kim, T. MacDougall, S..S. Vasu, H.J. Curran, A comprehensive experimental and improved kinetic modeling study on the pyrolysis and oxidation of propyne, Proc. Combust. Inst. 38 (2021).
[46] S. Dong, K. Zhang, P.K. Senecal, G. Kukkadapu, S.W. Wagnon, S. Barrett, N. Lokachari, S. Panigrahy, W..J. Pitz, H.J. Curran, A comparative reactivity study of 1-alkene fuels from ethylene to 1-heptene, Proc. Combust. Inst. 38 (2021).
[47] A. Ramalingam, S. Panigrahy, Y. Fenard, H. Curran, K.A. Heufer, A chemical kinetic perspective on the low-temperature oxidation of propane/propene mixtures through experiments and kinetic analyses, Combust. Flame 223 (2021) 361–375.
[48] Y. Sun, C.W. Zhou, K.P. Somers, H.J. Curran, An ab initio/transition state theory study of the reactions of C_5H_9 species of relevance to 1,3-pentadiene, Part I: potential energy surfaces, thermochemistry and high-pressure limiting rate constants, J. Phys. Chem. A 123 (2019) 9019–9052.
[49] Y. Sun, C.-.W. Zhou, K.P. Somers, H.J. Curran, An ab initio/transition state theory study of the reactions of C_5H_9 species of relevance to 1,3-pentadiene, Part II: pressure dependent rate constants and implications for combustion modelling, J. Phys. Chem. A 124 (2020) 4605–4631.
[50] J. Power, K.P. Somers, C.-.W. Zhou, S. Peukert, H.J. Curran, A theoretical, experimental and modeling study of the reaction of hydrogen atoms with 1- and 2-Pentene, J. Phys. Chem. A 123 (2019) 8506–8526.
[51] N. Lokachari, S. Panigrahy, G. Kukkadapu, G. Kim, S.S. Vasu, W.J. Pitz, H.J. Curran, The influence of iso-butene kinetics on the reactivity of di-isobutylene and iso-octane, Combust. Flame 222 (2020) 186–195.
[52] C.W. Zhou, Y. Li, U. Burke, C. Banyon, K.P. Somers, S. Ding, S. Khan, J.W. Hargis, T. Sikes, O. Mathieu, E.L. Petersen, M. AlAbbad, A. Farooq, Y. Pan, Y. Zhang, Z. Huang, J. Lopez, Z. Loparo, S.S. Vasu, H.J. Curran, An experimental and chemical kinetic modeling study of 1,3-butadiene combustion: ignition delay time and laminar flame speed measurements, Combust. Flame 197 (2018) 423–438.
[53] D.G. Goodwin, R.L. Speth, H.K. Moffat, B.W. Weber, Cantera: an object-oriented software toolkit for chemical kinetics, thermodynamics, and transport processes. https://www.cantera.org, doi:10.5281/zenodo.170284.
[54] Reaction-design, CHEMKIN-PRO 18.2, San Diego, 2013.
[55] S. Chih-Jen, H.J. Curran, Using rapid compression machines for chemical kinetics studies, Prog. Energy Combust. Sci. 44 (2014) 1–18.
[56] S.S. Goldsborough, S. Hochgreb, G. Vanhove, M.S. Wooldridge, H.J. Curran, S. Chih-Jen, Advances in rapid compression machine studies of low- and intermediate-temperature autoignition phenomena, Prog. Energy Combust. Sci. 63 (2017) 1–78.
[57] V. Gururajan, F.N. Egolfopoulos, Direct sensitivity analysis for ignition delay times, Combust. Flame 209 (2019) 478–480.
[58] X. Li, A.W. Jasper, J. Zádor, J.A. Miller, S.J. Klippenstein, Theoretical kinetics of $O + C_2H_4$, Proc. Combust. Inst. 36 (2017) 219–227.
[59] D.L. Baulch, C.T. Bowman, C.J. Cobos, R.A. Cox, Th. Just, J.A. Kerr, M.J. Pilling, D. Stocker, J. Troe, W. Tsang, R.W. Walker, J. Warnatz, Evaluated kinetic data for combustion modeling: supplement II, J. Phys. Chem. 34 (2005).
[60] H.P. Upadhyaya, A. Kumar, P.D. Naik, A.V. Sapre, Discharge flow reaction kinetic studies of $O(^3P)$ with chloroethylenes CH_2CCl_2, $CHClCCl_2$, CCl_2CCl_2, Chem. Phys. Lett. 321 (2000) 411–418.
[61] S.Y. Lee, H.S. Yoo, W.K. Kang, K.H. Jung, Reaction of $O(^3P)$ atoms with CF_2 = CXY (X, Y = H, F, C1, Br). Discharge flow-chemiluminescence imaging technique, Chem. Phys. Lett. 257 (1996) 415–420.
[62] S.E. Paulson, J.J. Orlando, G.S. Tyndall, J.G. Calvert, Rate coefficients for the reactions of $O(^3P)$ with selected biogenic hydrocarbons, Int. J. Chem. Kinet. 27 (1995) 997–1008.
[63] V.D. Knyazev, V.S. Arutyunov, V.I. Vedeneev, The mechanism of $O(^3P)$ atom reaction with ethylene and other simple olefins, Int. J. Chem. Kinet. 24 (1992) 545–561.
[64] O. Horie, R. Taege, B. Reimann, N.L. Arthur, P. Potzinger, Kinetics and mechanism of the reactions of $O(^3P)$ with SiH_4, CH_3SiH_3,$(CH_3)_2SiH_2$, and $(CH_3)_3SiH$, J. Phys. Chem. 95 (11) (1991) 4393–4400.
[65] D.M.V. Fonderie, J. Peeters, The kinetic coefficient of the C_2H_4+O reaction over extended pressure and temperature ranges, Physico-chemical behaviour of atmospheric pollutants, Springer, Dordrecht (1984), pp. 274–282.
[66] R.B. Klemm, J.W. Sutherland, M.A. Wickramaaratchi, G. Yarwood, Flash photolysis-shock tube kinetic study of the reaction of atomic oxygen (3P) with ethylene: 1052K.Itoreq. T.Itoreq.2284K, J. Phys. Chem. 94 (8) (1990) 3354–3357.
[67] K. Mahmud, P. Marshall, A. Fontijn, A high-temperature photochemistry kinetics study of the reaction of oxygen (3P) atoms with ethylene from 290 to 1510K, J. Phys. Chem. 91 (6) (1987) 1568–1573.
[68] T.L. Nguyen, L. Vereecken, X.J. Hou, M.T. Nguyen, J. Peeters, Potential energy surfaces, product distributions and thermal rate coefficients of the reaction of $O(^3P)$ with C_2H_4 (XAg): a comprehensive theoretical study, J. Phys. Chem. A 109 (33) (2005) 7489–7499.
[69] L.N. Krasnoperov, J.V. Michael, Shock tube studies using a novel multipass absorption Cell: rate constant results for OH + H_2 and OH + C_2H_6, J. Phys. Chem. A 108 (2004) 5643–5648.
[70] R. Sivaramakrishnan, J.V. Michael, B. Ruscic, High-temperature rate constants for H/D+ C_2H_6 and C_3H_8, Int. J. Chem. Kinet. 44 (3) (2012) 194–205.
[71] R. Sivaramakrishnan, C.F. Goldsmith, S. Peukert, J.V. Michael, Direct measurements of channel specific rate constants in OH + C_3H_8 illuminates prompt dissociations of propyl radicals, Proc. Combust. Inst. 37 (2019) 231–238.
[72] A.T. Droege, F.P. Tully, Hydrogen-atom abstraction from alkanes by hydroxyl. 3. Propane, J. Phys. Chem. 90 (1986) 1949–1954.
[73] A.W. Jasper, S.J. Klippenstein, L.B. Harding, Theoretical rate coefficients for the reaction of methyl radical with hydroperoxyl radical and for methylhydroperoxide decomposition, Proc. Combust. Inst. 32 (2009) 279–286.
[74] R. Zhu, C. Lin, The CH3 + HO2 Reaction: First-principles prediction of its rate constant and product branching probabilities, J. Phys. Chem. A 105 (2001) 6243–6248.

[75] Z. Hong, D.F. Davidson, K.-.Y. Lam, R.K. Hanson, A shock tube study of the rate constants of HO_2 and CH_3 reactions, Combust. Flame 159 (2012) 3007.
[76] S.J. Klippenstein, From Theoretical reaction dynamics to chemical modeling of combustion, Proc. Combust. Inst. 36 (2017) 77–111.
[77] J. Zádor, R.X. Fernandes, Y. Georgievskii, G. Meloni, C.A. Taatjes, J.A. Miller, The reaction of hydroxyethyl radicals with O_2: a theoretical analysis and experimental product study, Proc. Combust. Inst. 32 (2009) 271–277.
[78] J. Zador, S.J. Klippenstein, J.A. Miller, Pressure-dependent OH yields in alkene+HO_2 reactions: a theoretical study, J. Phys. Chem. A 115 (2011) 10218–10225.
[79] M.S. Stark, D.J. Waddington, Oxidation of propene in the gas phase, Int. J. Chem. Kinet. 27 (2) (1995) 123–151.